Two-gluon emission and interference in a thin QCD medium: insights into jet formation

Jorge Casalderrey-Solana,[a,b] Daniel Pablos[a] and Konrad Tywoniuk[a,c]

[a]*Departament d'Estructura i Constituents de la Matèria*
and Institut de Ciències del Cosmos (ICCUB),
Universitat de Barcelona, Martí i Franquès 1, 08028 Barcelona, Spain

[b]*Rudolf Peierls Centre for Theoretical Physics, University of Oxford,*
1 Keble Road, Oxford OX1 3NP, U.K.

[c]*Theoretical Physics Department, CERN,*
Geneva, Switzerland

E-mail: jorge.casalderreysolana@physics.ox.ac.uk, dpablos@ecm.ub.es,
konrad.tywoniuk@cern.ch

Abstract: In heavy-ion collisions, an abundant production of high-energy QCD jets allows to study how these multiparticle sprays are modified as they pass through the quark-gluon plasma. In order to shed new light on this process, we compute the inclusive two-gluon rate off a hard quark propagating through a color deconfined medium at first order in medium opacity. We explicitly impose an energy ordering of the two emitted gluons, such that the "hard" gluon can be thought of as belonging to the jet substructure while the other is a "soft" emission (which can be collinear or medium-induced). Our analysis focusses on two specific limits that clarify the modification of the additional angle- and formation time-ordering of splittings. In one limit, the formation time of the "hard" gluon is short compared to the "soft" gluon formation time, leading to a probabilistic formula for production of and subsequent radiation off a quark-gluon antenna. In the other limit, the ordering of formation is reverted, which automatically leads to the fact that the jet substructure is resolved by the medium. We observe in this case a characteristic delay: the jet radiates as one color current (quark) up to the formation of the "hard" gluon, at which point we observe the onset of radiation of the new color current (gluon). Within our kinematic constraints, our computation supports a picture in which the in-medium jet dynamics are described as a collection of subsequent antennas which are resolved by the medium according to their transverse extent.

Contents

1   Introduction

QCD jets are essential objects in modern particle physics. Many of the searches for new physics at the LHC involve the detailed analysis of the production and properties of these energetic spays of particles that arise from the colour neutralisation of energetic partons produced in hadronic collisions. Jets also play a central role in the analysis of hot and dense matter formed in the debris of high energy Pb-Pb collisions (for a recent review of LHC heavy-ion results see [1]). Since long, these objects have been identified as the most powerful tomographic tools with which to diagnose the properties of the formed matter [2]. The tremendous combined capabilities of the LHC (and its associated detectors) have converted this potential into reality; the copious production of jet samples at LHC energies enables detailed studies of jet properties in a heavy ion environment [3–18].

Early LHC results on jet physics in Pb-Pb collisions at $\sqrt{s_{\mathrm{NN}}} = 2.76\,\mathrm{TeV}$ have shown a strong suppression in the jet production rate as compared to proton-proton collisions at the same energies [15–17]. This reduction of the jet rate can be understood as a result of the energy loss experienced by jets on their way out of the collision zone. This phenomenon, known as jet quenching, was identified previously at RHIC by the observation of a strong suppression in the production of high energy hadrons in heavy ion collisions [19, 20]. While

the latter suppression is mostly sensitive to the energy loss by the hardest jet fragments, the variety of the observed jet modifications in a heavy-ion environment demands addressing the jets as sources of several partons propagating simultaneously through the QCD medium.

At high energies, parton energy loss is controlled by the stimulated radiation of medium-induced gluons as a result of the scattering with the medium constituents. Many of the properties of the modification of jets may be inferred from the single-gluon emission rate, first considered in [21] and computed by BDMPS-Z [22–24]. In a finite length medium, an opacity expansion of the multiple scattering series resummed in BDMPS-Z was introduced in [25–27], in which the expansion parameter may be viewed as the ratio of the medium length to the mean free path.[1] These computations are at the heart of the different formalisms later developed to address the dynamics of energetic partons in plasma [28–37]. Generalising this picture in order to treat the interactions of QCD showers with the medium, one usually relies on working models that iterate the single-gluon emission rate without considering possible multi-parton correlations. For different Monte-Carlo implementations, see [38–42]. Nevertheless, in vacuum jet physics it has been long understood that interference effects between the shower constituents, known as coherent branching or angular ordering, are essential to completely describe intra-jet properties in high-energy colliders [43].

For typical medium-induced gluons, all correlations are suppressed by the ratio of their formation time over the medium length [44], see also [45]. For large media, this allows to treat multiple medium-induced branchings in terms of a cascade [46, 47], see also [48, 49]. The large separation of scales, related in turn to the medium length and the mean free path, can also potentially lead to significant radiative corrections to transverse momentum broadening and energy loss in the medium [50–52] and, in general, to medium transport coefficients [51, 53]. See also [54, 55] for related work in next-to-leading order corrections to the medium-induced spectrum. The emission spectrum of two gluons with comparable formation times was analysed for the case of a dense medium in [56]. These approaches, however, consider the gluon transverse momenta to be of the order of the medium scale and therefore do not explicitly study the interplay between emissions of the former kind and genuine vacuum emissions, either short- or long-distance ones, which can take place in the context of high-energy jets. In the present work, we aim at providing further analytical insight into these situations, complementary to the numerical analysis of the rate at first order in medium opacity presented in [57].

The study of coherence effects for in-medium jets is a relatively new subject. In [58–63] the single gluon emission rate off two classical colour currents was computed in different approximations. The main finding of these studies may be summarised as the emergence of a new scale, the medium resolution scale, which controls the ability of the medium to resolve the number of colour emitters that traverse the plasma. If the transverse separation of the colour sources is larger than this scale, the medium is able to interact independently with each of the sources, and the medium-induced radiation spectrum consists of the superposition of the induced spectrum from each of the colour currents. If the transverse

---

[1]This ratio is usually referred to as the medium opacity.

separation is small compared to this scale, the system interacts coherently with the propagating currents and the medium-induced spectrum coincides with that of a single colour charge in the overall colour representation of the system of currents. The phenomenon of medium resolution has also been recently found in the dynamics of energetic colour objects plunging through infinitely strongly coupled gauge theory plasmas [64]. These findings lead to the suggestion of a new picture for jet dynamics in heavy-ion collisions where, from the point of view of the medium, the jet shower is organised in terms of effective emitters, according to the medium resolution scale [65].

In this paper we study the coherent branching of soft gluons in jet showers by directly analysing the double-inclusive gluon emission rate. The two gluons have well separated energies, which are both much smaller than the quark energy. We will model the interaction of the jet with hadronic matter by a single in-medium exchange, which occurs at a given distance from the hard production vertex that generates the shower. This medium model corresponds to the leading order of an opacity expansion for a medium which can be situated at any distance from the hard vertex. In the lowest order opacity expansion approach, one performs the integral over the position of the scattering centres, thus arriving at sequential interactions that add to the average number of scattering centres along the jet path. In this paper we do not perform this integral. The so called $N = 1$ opacity approximation has been very successful in describing different aspects of hard probes in heavy ion collisions, (see, for example, [66–70]; for other perturbative-based analyses of fully reconstructed jets see, for example [71–76]). Nevertheless, we will consider this approximation as a working model with which to understand jet-medium interactions. In particular, we will place the in-medium exchange at will and use its a a chronometer, which tests the jet shower at different times. The double inclusive emission rate in the $N = 1$ opacity approximation was analysed in [57] for fixed values of the medium parameters. However, our computation is not aimed at describing the gluon emission rate in a realistic model of the hot matter produced in ultra-relativistic heavy-ion collisions but rather to understand how in-medium interactions generically affect the gluon radiation pattern.

2 Preliminaries

We compute the inclusive rate off a hard quark that emits two soft gluons while it interacts with a single coloured exchange. In the absence of scattering centres, those gluons originate from the relaxation of virtuality of the microscopic process that generates the energetic quark. The presence of such a single gluon exchange leads to a modification of the vacuum spectrum by changing the transverse momentum of one of the gluons emitted at the production vertex. In addition, the additional momentum transferred to the jet supplemented by the medium leads to an additional source of radiation of gluons with transverse momentum of the order of the momentum transfer. This process is the stimulated emission of gluons in the medium. We explicitly study the effect of interferences among these different physics processes in the final emission rate. We will work in light-cone coordinates $X = (x^+, x^-, \boldsymbol{x})$, where $x^\pm \equiv (x^0 \pm x^3)/2$ and $\boldsymbol{x} = (x_1, x_2)$ denotes a transverse vector, $x \equiv |\boldsymbol{x}|$. For future reference, the momenta of the quark, the "hard" and the "soft" gluons are given by $P = (p^+, 0, \boldsymbol{0})$, $K_H = (k_H^+, k_H^-, \boldsymbol{k}_H)$ and $K_S = (k_S^+, k_S^-, \boldsymbol{k}_S)$, respectively.

2.1 Medium model

As the partons produced in a jet shower plough through a QCD medium, they exchange energy and momentum with its constituents. Since these interactions are mediated by the exchange of gluons, an effective way to encode those interactions is by analysing the propagation of energetic partons in a fluctuating colour gauge field, A, sourced by the quarks and gluons in the medium. For high-energy probes, the light-cone gauge $A^+ = 0$, with the plus-momentum component the largest momentum of the parton, is particularly convenient. In this gauge, typical fluctuating fields in the background will have all other components of comparable order. Since in the eikonal limit, which we will briefly describe in the next subsection, the coupling of a parton of momentum P^μ to the medium gauge field is proportional to $P \cdot A$, the contribution of the perpendicular field components A^i to the probe-medium interactions is suppressed with respect to the contribution of the A^- component.

The high-energy approximation also leads to simplifications in the momentum exchange with the medium. Assuming that the p^+ component of the probe is much larger than the momentum exchanged in the medium, q, the effect of the q^+ exchanged momentum is always suppressed with respect to the transverse momentum exchanges, $\boldsymbol{q}$, since by energy momentum conservation in the vertex the former is always added to the large parton momentum. This is equivalent to neglecting drag ($q^+ \approx 0$) for high-energy probes. With these assumptions, we can model the medium by a gauge field with only one non-vanishing component, which takes the form

$$A^-(Q) \equiv t^a A^{a,-}(Q) = 2\pi\delta(q^+) \int \mathrm{d}x^+ e^{iq^- x^+} \mathcal{A}(x^+; \boldsymbol{q}), \qquad (2.1)$$

where $Q = (q^+, q^-, \boldsymbol{q})$ and the medium field is real, $\mathcal{A}^*(x^+; \boldsymbol{q}) = \mathcal{A}(x^+; -\boldsymbol{q})$.

The medium dynamics leads to the randomisation of the field. From the point of view of the probe, we may characterise the medium by cumulants of the fluctuating field configurations. Odd cumulants vanish as a consequence of colour neutrality of the medium. Even n-point medium correlators exhibit correlation lengths of order the inverse medium exchange. This allows us to approximate the medium average of the background gauge field to

$$\langle \mathcal{A}^a(x^+; \boldsymbol{q}) \mathcal{A}^{*b}(x'^+; \boldsymbol{q}') \rangle = \delta^{ab} m_D^2 n(x^+) \, \delta(x^+ - x'^+) \, (2\pi)^2 \delta(\boldsymbol{q} - \boldsymbol{q}') \mathcal{V}^2(\boldsymbol{q}), \qquad (2.2)$$

where $n(x^+)$ is the density of scattering centres in the x^+ direction [77]. In the simplest of cases, a static medium with fixed density n_0 and length L, $n(x^+) = n_0\Theta(L - x^+)$. As a consequence of Lorentz contraction, the correlation length along the x^+ direction can be neglected and we may consider exchanges as instantaneous in x^+. Furthermore, $\mathcal{V}(\boldsymbol{q})$ is the scattering potential, usually assumed to be screened at the scale of the Debye mass m_D. However, in our discussion the exact form of this potential does not matter as long as it is *isotropic* in the transverse plane.

The locality in x^+ of the correlator eq. (2.2) also implies that higher-order cumulants vanish in this high-energy approximation, such that higher-order medium correlators are

simply products of the two point functions eq. (2.2). The $N = 1$ opacity approximation consists in describing all medium effects by the two point function eq. (2.2). This is a good approximation when the medium is dilute, $\alpha_s n_0 L \ll 1$. If the medium is dense, a re-summation of an arbitrary number of medium exchanges is required. Nevertheless, in this paper we will employ the $N = 1$ opacity approximation as a tool to explore the dynamics of energetic jet showers in QCD medium, but we will make no assumptions on whether this approximation correctly captures the properties of the quark-gluon plasma formed in heavy-ion collisions.

2.2 Computing the amplitude and cross section

In our computation we assume the following energy ordering $p^+ \gg k_H^+ \gg k_S^+$. This is the conventional ordering of a vacuum shower leading to the double-logarithmic enhancement of gluon emissions. In the presence of the medium, such an ordering allows us to study how the hard jet substructure builds up in the presence of a probing, soft gluon which can be either collinear or medium-induced.

We also assume that the energy of both gluons is much larger than the typical momentum transfer from a medium exchange q, $k_S^+ \gg q$. In order to consistently neglect the radiation from the scattering centre, we will focus solely on collinear emissions with respect to the quark; this means that the emission angles of both of the gluons, $\theta_H = k_H/k_H^+$ and $\theta_S = k_S/k_S^+$, are small. However, we will make no assumptions about the relative magnitude of the emission angles θ_H/θ_S. To account for all relevant medium effects, we will allow the transverse momentum of one of the gluons, k_S, to be of the order of the in-medium momentum transfer q.

These assumptions simplify significantly the computation of the emission amplitudes. Since we are focusing in the rate in which both the gluons and the quark possess a much larger energy than the medium momentum transfer, we can use an eikonal approximation for the QCD Feynman rules that allows us to exploit this separation of scales at amplitude level. For ease of computation we will work in the mixed representation where the minus-component of the momenta is Fourier transformed to configuration space. Although the eikonal Feynman rules are well-known, we have re-derived them in appendix A to clearly state our approximations and for the readers convenience. To discuss how we have organised our computation, we proceed to list the main ingredients.

In the eikonal limit, the quark and triple-gluon vertices conserve spin and helicity, respectively. It is useful to absorb the spin and polarization of the propagating degrees of freedom of adjacent propagators into properly contracted vertices, see appendix A. In this way the amplitude can be defined in terms of spin and polarisation independent vertices and propagators. In our present calculations, we will be using two types of eikonal emission vertices which are justified by the ordering of energies we have assumed. First, emissions of gluons off the energetic quark come with the factor

$$V_G^{a,i}(p^+; \boldsymbol{k}_I, k_I^+) \equiv V_G^{a,i}(\boldsymbol{0}, p^+; \boldsymbol{k}_I, k_I^+) = 2ig\, t^a \frac{p^+}{k_I^+}\, k_I^i\,, \qquad (2.3)$$

where $I = H, S$, while the gluon splitting brings a factor

$$\Gamma_G^{abc,i}(\boldsymbol{k}_H, k_H^+; \boldsymbol{k}_S, k_S^+) = 2g\, f^{abc} \frac{1}{z} \kappa_S^i\,, \qquad (2.4)$$

where we have defined $z \equiv k_S^+/k_H^+$ and

$$\boldsymbol{\kappa}_S \equiv \boldsymbol{k}_S - z\,\boldsymbol{k}_H \tag{2.5}$$

is the relative momentum of the emission. Both effective vertices are transverse vectors and are proportional to the relevant colour factor. The four-gluon vertex does not exhibit the $1/z$ enhancement of eq. (2.4), and it is therefore negligible in this kinematic limit. The same argument holds for the gluon splitting into a quark-antiquark pair.

The momentum in eq. (2.5) deserves some discussion. Naively, the strong ordering in the energy of the gluon suggests that we may drop the apparently subleading contribution $z\boldsymbol{k}_H$ in the definition of $\boldsymbol{\kappa}_S$. However, this can only be done if $\boldsymbol{k}_H$ and $\boldsymbol{k}_S$ are of the same order. This is the case when both gluons are medium-induced. However, in this paper we will be interested in exploring the emission rate when the angles in transverse space θ_H and θ_S are comparable, which implies that k_H is parametrically (in $1/z$) larger than k_S.

Since there is only one non-vanishing component of the medium potential, the effective interaction vertices become scalars, and read

$$u_Q^a(p^+) = 2ig\,t^a\,p^+\,, \tag{2.6}$$
$$u_G^{abc}(p^+) = 2g\,f^{abc}\,p^+\,, \tag{2.7}$$

where we have amputated the medium field in the definition of the vertex; for details see appendix A.

Having absorbed all spinor and helicity structures into the vertices, the internal partons are simply described by scalar propagators. Keeping the leading energy correction on the position of the poles, the propagation of the gluons in the mixed representation, see eq. (A.9), may be expressed as

$$D_G(x^+; \boldsymbol{k}_I, k_I^+) \equiv D(x^+; \boldsymbol{k}_I, k_I^+) = \frac{\Theta(x^+)}{2k^+} \exp\left[-i\frac{\boldsymbol{k}_I^2}{2k_I^+}x^+ - \epsilon x^+\right]\,, \tag{2.8}$$

where again $I = H, S$ and $\Theta(x)$ is the Heaviside theta-function. The propagation of the quark is identical to that of the gluon; however, since we are taking the quark to have a much larger energy, we will adopt the strict eikonal limit, $k_H/p^+, k_S/p^+, q/p^+ \ll 1$,

$$D_Q(x^+; p^+) \equiv D(x^+; \boldsymbol{0}, p^+) = \frac{\Theta(x^+)}{2p^+} e^{-\epsilon x^+}\,. \tag{2.9}$$

The ϵ-prescription in the propagators above suppresses the propagation of modes in the distant past and future. Finally, all in-coming and out-going particles have to be multiplied by the appropriate phases, embodying energy-momentum conservation, and by spinor or polarization vectors for quarks and gluon, respectively; see appendix A for more details.

These eikonal rules are the building blocks with which we construct the double gluon emission rate. Neglecting the four-gluon vertex, the full computation of this process involves the calculation of 15 real amplitudes, summarised in Figs 1 and 3. Also, a total 23 additional non-vanishing virtual corrections, or double-Born diagrams, which involve the interference between double scattering amplitudes with vacuum diagrams, need to be
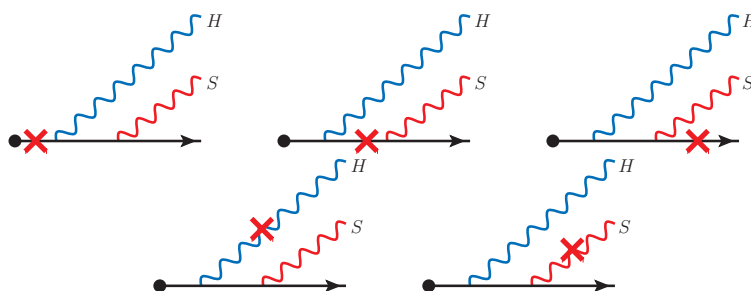
Figure 1. Two-gluon emission off a quark with $N = 1$ interactions with the medium. We also include the diagrams with the substitution $H \leftrightarrow S$.
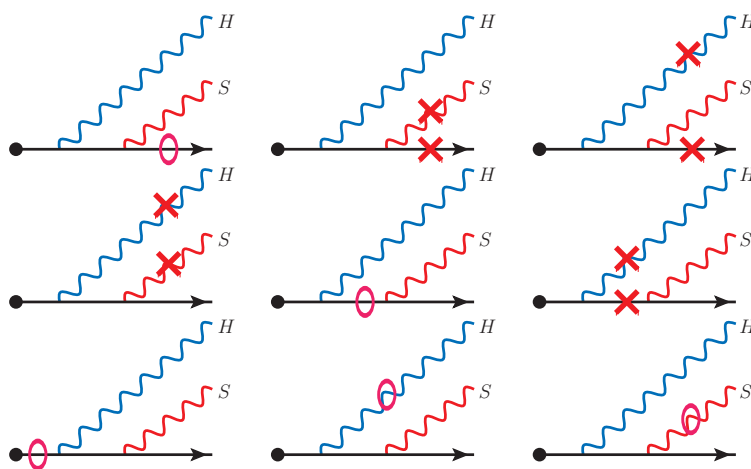
Figure 2. Two-gluon emission off a quark with $N = 1$ unitarity corrections. We also include the diagrams with the substitution $H \leftrightarrow S$.
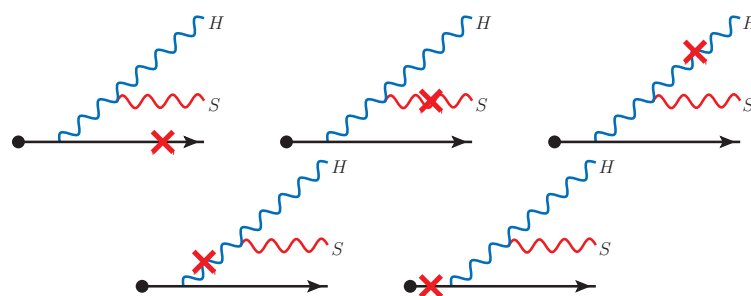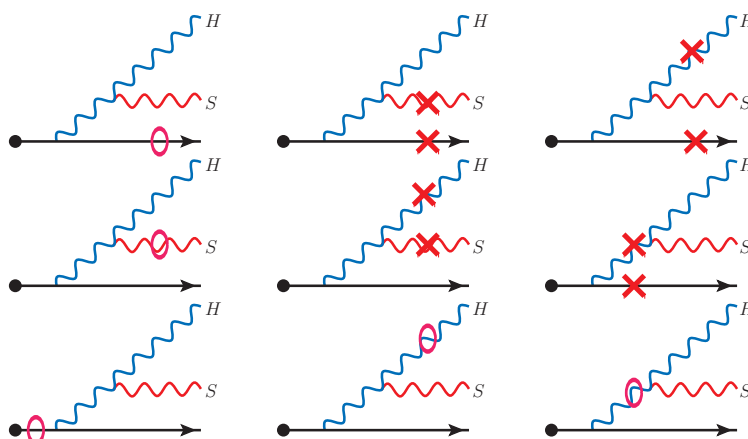

Figure 3. Sequential two-gluon emission off a quark and with $N = 1$ interactions with the medium.

considered. These are summarised in figures 2 and 4. All relevant Feynman rules are summarised in appendix A.3. After squaring the real diagrams, the full rate is composed of 248 combinations.

Given the large number of diagrams that needs to be computed and squared, in this paper we have used an automated procedure to compute this cross section. We have coded

Figure 4. Sequential two-gluon emission off a quark with $N = 1$ unitarity corrections.

the Feynman rules outlined in the previous section in Mathematica, where we perform all integrations, sums and colour algebra via symbolic computations. The amplitude of these processes can be written as

$$\mathcal{M}^{ab}_{(0)\,\lambda\lambda'} = \varepsilon^i_\lambda(\boldsymbol{k}_H)\varepsilon^j_{\lambda'}(\boldsymbol{k}_S)\sum_k m^{ab,ij}_k\,, \tag{2.10}$$

$$\mathcal{M}^{ab}_{(1)\,\lambda\lambda'} = \int_{x^+}\int_{\boldsymbol{q}}\varepsilon^i_\lambda(\boldsymbol{k}_H)\varepsilon^j_{\lambda'}(\boldsymbol{k}_S)\mathcal{A}^c(x^+;\boldsymbol{q})\sum_k m^{abc,ij}_k(x^+;\boldsymbol{q})\,, \tag{2.11}$$

$$\mathcal{M}^{ab}_{(2)\,\lambda\lambda'} = \int_{x^+.x'^+}\int_{\boldsymbol{q},\boldsymbol{q}'}\varepsilon^i_\lambda(\boldsymbol{k}_H)\varepsilon^j_{\lambda'}(\boldsymbol{k}_S)\mathcal{A}^c(x^+;\boldsymbol{q})\mathcal{A}^d(x'^+;\boldsymbol{q}')\sum_k m^{abcd,ij}_k(x^+,x'^+;\boldsymbol{q},\boldsymbol{q}')\,, \tag{2.12}$$

where the basic building blocks are the amputated amplitudes $m^{abXY,ij}_k(\ldots)$. The first two superscripts $\{a, b\}$ relate to the colour structure and the latter two $\{i, j\}$ relate to the indices of the two out-going transverse momenta, with $\{\lambda, \lambda'\}$ being their respective polarizations. The superscripts X and Y and the number of arguments relate to the number of insertions of the medium field. In the argument of the function we have suppressed the kinematics of the emitted gluon. The subscript k simply designates the particular diagram under consideration, and the sum runs over all diagrams in figures 1 and 3 for eq. (2.11) and figures 2 and 4 for eq. (2.12). The vacuum terms are also trivially found from these diagrams. Thus, eq. (2.10) is the sum of all vacuum amplitudes, eq. (2.11) is the sum of diagrams with one medium insertion, and eq. (2.12) is the sum of all non-vanishing amplitudes with two medium insertions. We will refer to $\mathcal{M}_{(1)}$ as medium-real diagrams, and $\mathcal{M}_{(2)}$ will be referred to as medium-virtual diagrams.

Of course, all the amplitudes in eqs. (2.10)–(2.12) are also proportional to the amplitude of the hard process that created the out-going quark. Since this simply factorises into the Born cross-section for quark production, we will always suppress it.

To illustrate the procedure, we describe here how to compute one of the amputated amplitudes, namely the upper left diagram of figure 1, which reads

$$
m_1^{abc,ij}(x^+; \boldsymbol{q}) = \int_{x_H^+, x_S^+} e^{ik_H^- x_H^+ + ik_S^- x_S^+} V_G^{a,i}(p^+; \boldsymbol{k}_H, k_H^+) D_Q(x_S^+ - x_H^+; p^+)
$$
$$
\times V_G^{b,j}(p^+; \boldsymbol{k}_S, k_S^+) D_Q(x_H^+ - x^+; p^+) u_Q^c(p^+) D_Q(x^+ - x_0^+; p^+), \quad (2.13)
$$

where the gluons are on-shell: $k_H^- = \boldsymbol{k}_H^2/(2k_H^+)$ and $k_S^- = \boldsymbol{k}_S^2/(2k_S^+)$. In order to alleviate the notation, we have also defined the integrals

$$
\int_{x^+} = \int_{-\infty}^{\infty} \mathrm{d}x^+ , \qquad (2.14)
$$

$$
\int_{\boldsymbol{q}} = \int \frac{\mathrm{d}^2 \boldsymbol{q}}{(2\pi)^2} , \qquad (2.15)
$$

and usually we will set $x_0^+ = 0$ if not stated otherwise.

In this amputated amplitude, i and j are transverse space indices that denote the transverse momentum component of the soft and hard gluons, while a and b are their respective colour indices. The positions x_H^+, x_S^+ and x^+ denote the position in configuration space where the hard and soft emissions and the scattering with the medium take place. Finally, the two phase factors appearing in the integrand are a consequence of the external leg insertion. To deal with the colour algebra we use the ColorMath package [78].

Following these simple rules, we introduce all amplitudes in Mathematica, which we also use to square them. The x_H^+ and x_S^+ integrals in the amputated amplitude, see eq. (2.13), and the transverse momentum multiplication are performed symbolically. Formally, we take advantage of the medium average eq. (2.2) to write for the square of the medium-real amplitudes

$$
\langle |\mathcal{M}_{(1)}|^2 \rangle = \int_{x^+, x'^+} \int_{\boldsymbol{q}, \boldsymbol{q}'} \langle \mathcal{A}^c(x^+; \boldsymbol{q}) \mathcal{A}^{*\,c'}(x'^+; \boldsymbol{q}') \rangle \sum_{k,k'} m_{(k)}^{abc,ij}(x^+; \boldsymbol{q}) m_{(k')}^{*abc',ij}(x'^+; \boldsymbol{q}')
$$
$$
= m_D^2 \int_{x^+} \int_{\boldsymbol{q}} n(x^+) \mathcal{V}(\boldsymbol{q})^2 \sum_{k,k'} m_{(k)}^{abc,ij}(x^+; \boldsymbol{q}) m_{(k')}^{*abc,ij}(x^+; \boldsymbol{q}) , \qquad (2.16)
$$

where the sum of all repeated indices is assumed and we have used $\sum_\lambda \varepsilon_\lambda^i(\boldsymbol{k}) \varepsilon_\lambda^j(\boldsymbol{k}) = \delta^{ij}$ in order to contract the transverse indices. A similar strategy can be followed for the medium-virtual amplitudes, which are added by multiplying them with the vacuum amplitudes such that

$$
\langle \mathcal{M}_{(2)} \mathcal{M}_{(0)}^* \rangle = \int_{x^+, x'^+} \int_{\boldsymbol{q}, \boldsymbol{q}'} \langle \mathcal{A}^c(x^+; \boldsymbol{q}) \mathcal{A}^{c'}(x'^+; \boldsymbol{q}') \rangle \sum_{k,k'} m_{(k)}^{abcc',ij}(x^+, x'^+; \boldsymbol{q}, \boldsymbol{q}') m_{(k')}^{*ab,ij}
$$
$$
= m_D^2 \int_{x^+} \int_{\boldsymbol{q}} n(x^+) \mathcal{V}(\boldsymbol{q})^2 \sum_{k,k'} m_{(k)}^{abcc,ij}(x^+, x^+; \boldsymbol{q}, -\boldsymbol{q}) m_{(k')}^{*ab,ij} . \qquad (2.17)
$$

In particular, when calculating contact terms (i.e. diagrams with two insertions on the same propagator, denoted with a circle in figures 2 and 4) we use the half-value prescription for

the Heaviside function, $\Theta(0) = 1/2$, which yields the correct answer for the double-Born diagrams (for a detailed derivation of the contribution of these diagrams, see [27]). The full medium-induced spectrum at first order in opacity is then

$$\langle|\mathcal{M}_{1\mathrm{OP}}|^2\rangle = \langle|\mathcal{M}_{(1)}|^2\rangle + 2\mathrm{Re}\langle\mathcal{M}_{(2)}\mathcal{M}_{(0)}^*\rangle$$
$$= m_D^2 \int_{x^+} \int_{\boldsymbol{q}} n(x^+)\mathcal{V}^2(\boldsymbol{q})\, w(x^+;\boldsymbol{q})\,, \qquad (2.18)$$

where

$$w(x^+;\boldsymbol{q}) = \sum_{k,k'} \Big[m_{(k)}^{abc,ij}(x^+;\boldsymbol{q})m_{(k')}^{*abc,ij}(x^+;\boldsymbol{q}) + m_{(k)}^{abcc,ij}(x^+,x^+;\boldsymbol{q},-\boldsymbol{q})m_{(k')}^{*ab,ij}$$
$$+ m_{(k)}^{ab,ij}m_{(k')}^{*abcc,ij}(x^+,x^+;\boldsymbol{q},-\boldsymbol{q}) \Big]\,. \qquad (2.19)$$

The spectrum of emitted gluons is then

$$\frac{\mathrm{d}^2 N_{1\mathrm{OP}}}{\mathrm{d}\Omega_{k_H}\,\mathrm{d}\Omega_{k_S}} \equiv \frac{1}{\sigma_q^{\mathrm{Born}}} \frac{\mathrm{d}^2\sigma_{1\mathrm{OP}}}{\mathrm{d}\Omega_{k_H}\,\mathrm{d}\Omega_{k_S}} = \frac{1}{2p^+}\langle|\mathcal{M}_{1\mathrm{OP}}|^2\rangle\,, \qquad (2.20)$$

where the factor $1/(2p^+)$ is the quark flux and the phase space for the gluons is given by $\mathrm{d}\Omega_k \equiv (2\pi)^{-3}\mathrm{d}^2\boldsymbol{k}\,\mathrm{d}k^+/(2k^+)$. Unitarity implies that the full $\langle|\mathcal{M}_{1\mathrm{OP}}|^2\rangle \to 0$ when the medium momentum exchange vanishes, $q \to 0$. We have explicitly checked that our expressions respect this condition, which for the particular case at hand it implies an exact cancellation of medium-real and medium-virtual diagrams takes place in this limit, such that no double-counting with the pure vacuum cross section occurs.

3 Analysis of the induced rate

The strategy of computing the full amplitude in an automatised form allows us to deal with the many diagrams we have computed in a simple and effective way. However, the answer that this computation yields is lengthy and we have not been able to reduce it to a simple form. Therefore, in this section we will explore two particularly interesting limits of this expressions in which we have managed to express the answer in a closed form. This analysis is complementary to the numerical analysis of the full rate performed in [57].

Prior to taking these two limits, some general considerations about the full square matrix are in order. The analysis of the colour structure of both the real and virtual contributions allows us to separate the full answer into only two non-vanishing colour structures (after averaging over colours). The total rate may be expressed as

$$w(x^+;\boldsymbol{q}) = C_F^2 C_A w_Q(x^+;\boldsymbol{q}) + C_F C_A^2 w_G(x^+;\boldsymbol{q})\,, \qquad (3.1)$$

where the elements w_Q and w_G are functions of the kinematic variables. This general structure admits a simple interpretation. The full rate may be understood as the sum of two different physical processes: i) the emission of two gluons off the high-energy quark, w_Q; and ii) the emission of a hard gluon off the high-energy quark which, in turn, emits an

additional soft gluon w_G. These emissions can occur either as originated from the initial virtuality of the hard vertex that creates the energetic quark or as a result of the interaction of the system with the medium. Note that in the infinite quark energy limit, the change of momentum of the quark as a result of the interaction and emission processes is negligible. This implies that, effectively, only the gluon scatters and terms proportional to C_F^3 are suppressed by powers of the quark energy.

The expressions for w_Q and w_G may also be organised according to their dependence on the position of the colour exchange, x^+. In general, we can express these two terms as

$$w_I(x^+; \boldsymbol{q}) = \sum_{i=1}^{N_I} \mathcal{P}_I^{(i)}(\boldsymbol{q})\Big\{1 - \cos\big[x^+/\tau_I^{(i)}(\boldsymbol{q})\big]\Big\} \tag{3.2}$$

where $I = Q, G$, $N_Q = 2$ and $N_G = 19$ is the number of independent terms for the two distinct colour structures and the functions $\mathcal{P}_Q^{(i)}$, $\mathcal{P}_G^{(i)}$, $\tau_Q^{(i)}$, $\tau_G^{(i)}$ are rational functions of products of the four momenta of the three partons as well as of the transferred momenta. These are, in general, complicated expressions which we have not been able to simplify to a compact form, and shall therefore not be presented here. In the following subsections we will show instead the results obtained by the consideration of two distinct kinematic limits.

It is interesting to note that all the dependence of the full rate, eq. (3.2), on the position of the colour exchange, x^+, occurs in the form of cosine-like phase factors. These phases indicate interference effects between the vacuum production of the quark, at $x_0^+ = 0$, and the medium scattering processes. For single gluon emission these interferences are well known, and are the precursors of the Landau-Pomeranchuk-Migdal (LPM) effect. In the context of radiation induced by a single exchange, this effect can be understood as the frustration of the induced radiation when the scattering occurs too close to the hard vertex, at a distance shorter than the formation time of the emitted gluon, $\tau = 2k^+/(\boldsymbol{k}-\boldsymbol{q})^2$. While in the single emission rate all the cross section is characterised by this single time-scale, in the double-gluon emission rate several time-scales appear.

This distinct x^+ dependence of the total rate allows us to treat differently the kinematic factors $\mathcal{P}_I^{(i)}$ and the formation factors $\tau_I^{(i)}$ when expanding the rate in different kinematic regions. The limits we will explore invoke certain assumptions about the momenta of the partons and the transferred momenta, for *any* medium length L. In fact, the dependence of any scale related to the medium length only enters in the computation via the phase factors, as L appears in the limits of integration of x^+. Therefore, interferences are solely dependent on the relative magnitude of the formation factor $\tau_I^{(i)}$ and the medium length. For this reason, when taking kinematic limits, it is consistent to expand the kinematic factors $\mathcal{P}_I^{(i)}$ and $\tau_I^{(i)}$ to different orders since apparently subleading terms in $\tau_I^{(i)}$ may be enhanced by the medium length. In the next two subsections we will specify the limits we explore and describe this approximation in more detail.

3.1 Expansion parameters

We now specify the parameters which we use to expand the symbolically computed cross section. First of all, as it is clear from the Feynman rules in section 2.2, the energy

of the quark disappears from the final rate, since there is a cancellation between the p^+-dependence of the eikonal vertices and the eikonal quark propagators. This is only true in the strictly infinite quark energy limit that we adopt. Secondly, the structure of these rules also indicates that the rate depends on the energies of both emitted gluons via the combination

$$z = \frac{k_S^+}{k_H^+}, \tag{3.3}$$

which, by assumption, is small.

We analyse the double emission rate as a function of the emission angles of the two gluons. Assuming both these angles are small, these are trivially related to the momentum of the emitted gluons via

$$\theta_H = \frac{k_H}{k_H^+}, \qquad \theta_S = \frac{k_S}{k_S^+}. \tag{3.4}$$

In terms of these angles, the variable κ_S, defined in eq. (2.5), is independent of z. To make this scaling explicit, we may write κ_S as

$$\kappa_S = k_S^+ \left(\theta_S \, \mathbf{n}_S - \theta_H \, \mathbf{n}_H \right) \tag{3.5}$$

with $\mathbf{n}_S$ ($\mathbf{n}_H$) the unit transverse vector along the direction of $\boldsymbol{k}_S$ ($\boldsymbol{k}_H$). This form motivates us to organise the computation in terms of the (dimensionless) ratio of angles

$$r = \frac{\theta_H}{\theta_S}. \tag{3.6}$$

In addition to the momenta of both gluons, the medium interaction introduces an additional dimension-full quantity, namely the momentum transferred by the medium, $\boldsymbol{q}$. In order to properly take limits of the full rate, we need to consider the relative magnitude of this momentum transfer to other dimension-full quantities in the rate. Motivated by the fact that the single-gluon medium-induced rate is dominated by gluons with transverse momenta of order the transferred momentum, we choose to organise our computation in terms of the (dimensionless) ratio

$$\tilde{q} = \frac{q}{k_S} = \frac{1}{z\theta_S} \frac{q}{k_H^+}. \tag{3.7}$$

This ratio ensures that, as long as we keep $\tilde{q}$ finite, the softest gluon in the amplitude may be medium-induced. This choice of scaling introduces a non-trivial dependence of the emission rate on the variable z. This may be best illustrated by considering the ratio between the transferred momentum and the transverse momentum of the hard gluon

$$\frac{q}{k_H} = \tilde{q} \frac{z}{r}. \tag{3.8}$$

Although by construction we have assumed that z is small in the Feynman rules, the introduction of the scaling eq. (3.7) leads to a different behavior depending on the relative
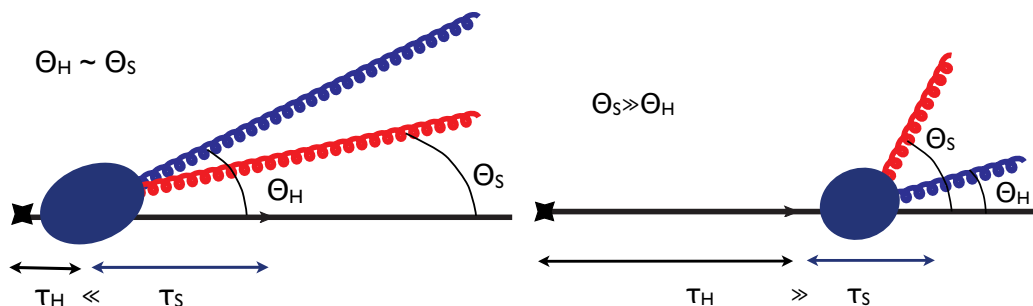
Figure 5. Sketch of the two kinematic limits of the double emission rate considered in this paper. In both panels the hard gluon is blue while the soft gluon is red and the blob represents all possible placements of the in-medium exchange. The soft limit is represented in the left panel; in this limit the formation time of the hard gluon is very short compared to the soft gluon one and the angles of emission of both gluons are comparable. In the collinear limit, right panel, the angle of emission of the hard gluon is very small and its formation time is long compared to the soft gluon formation time.

magnitude of z and r. By keeping $\tilde{q}$ fixed, the limit $z \ll r$ implies that the transverse momentum of the hard gluon is much greater than the medium momentum transfer; complementary, for the limit in which $r \ll z$ the transverse momentum of the hard gluon is much smaller than the momentum transfer. These are the two limits that we will explore in the next subsection. We will leave the analysis of the region $r \sim z$, in which the transverse momentum of both gluons are comparable to the medium transfer, for future work.

These two particular limits also have a close relation to two distinct space-time pictures of the emissions. In the limit of small z, the hard gluon is formed early in the medium. The two hardest partons, the quark and the hard gluon, will therefore form an effective dipole, or antenna, that is probed by the emission of the softest parton in the cascade. This situation is close in spirit to the one studied in [58–63]. In the opposite limit, the formation times of the soft gluon is shorter than the hard one, allowing it to be emitted earlier in the cascade. This is a novel situation that we study for the first time in detail.

3.2 Emission rate in the soft limit

We start by studying the double induced gluon rate in the limit $z \ll r$, i. e.,

$$z \to 0, \quad \text{with} \quad \left\{ r, \tilde{q}, \theta_S, k_H^+ \right\} \text{ fixed}. \tag{3.9}$$

As already discussed, in this limit eq. (3.8) implies that k_H decouples from the medium scale. This means that the medium-induced rate of the hard gluon is power suppressed and, to leading order in z, the rate of emission of this gluon is dominated by the vacuum processes associated to the hard vertex. Note also that the (vacuum) formation times of the two gluons are strongly ordered,

$$\frac{\tau_H}{\tau_S} = \frac{z}{r^2}, \tag{3.10}$$

with $\tau_H = 2k_H^+/\boldsymbol{k}_H^2$ and $\tau_S = 2k_S^+/\boldsymbol{k}_S^2$ the vacuum formation times of the hard and soft gluons, respectively. Therefore, at leading order in z, the hard gluon is effectively emitted

from the hard vertex since it is formed at an arbitrarily short time. A sketch of this limit can be found in figure 5 left.

We expand the prefactors $\mathcal{P}_Q^{(i)}$ and $\mathcal{P}_G^{(i)}$ in eq. (3.2) to leading order in z, which means that we only keep terms that diverge as z^{-2}. In this limit, only 1 out of the 2 $\mathcal{P}_Q^{(i)}$ and 10 out of the total 19 $\mathcal{P}_G^{(i)}$ terms remain. The phase factors of those terms, $\tau_Q^{(i)}$ and $\tau_G^{(i)}$, possess different leading z behavior, z^{-1}. Following the discussion around eq. (3.2) (on the presence of a new scale, the position of the colour exchange from the hard vertex, x^+) induces us to expand the phase factors $\tau_Q^{(i)}$, $\tau_G^{(i)}$ to a different z-order than the prefactors $\mathcal{P}_Q^{(i)}$ and $\mathcal{P}_Q^{(i)}$. Performing this limit, several cancellations occur and we ultimately were able to bring the cross section to a closed form.

Following the notation of eq. (3.1), the term associated to the emission of the two gluons by the quark, proportional to the colour factor $C_F^2 C_A$, is in the leading z-limit given by

$$w_Q(x^+; \boldsymbol{q}) = \frac{4g^2}{\boldsymbol{k}_H^2} \times \left(-8g^4\right) \frac{\boldsymbol{k}_S \cdot \boldsymbol{q}}{(\boldsymbol{k}_S + \boldsymbol{q})^2 \, \boldsymbol{k}_S^2} \left\{ 1 - \cos\left[\frac{(\boldsymbol{k}_S + \boldsymbol{q})^2}{2k_S^+} x^+ \right] \right\}, \qquad (3.11)$$

where we have expressed all the factors in terms of products of the final momenta. This expression admits a simple physical interpretation. This part of the cross section is the product of the vacuum probability of emitting a gluon off the hard quark (in the soft limit), $\sim 1/\boldsymbol{k}_H^2$, times the $N = 1$ opacity spectrum for the medium-induced emission of a soft gluon by the same quark [25, 26]. For later convenience, let us define the vectors,

$$\boldsymbol{A}_q = \frac{\boldsymbol{k}_S + \boldsymbol{q}}{(\boldsymbol{k}_S + \boldsymbol{q})^2}, \quad \boldsymbol{B}_q = \frac{\boldsymbol{k}_S}{\boldsymbol{k}_S^2}, \quad \boldsymbol{L}_q = \boldsymbol{A}_q - \boldsymbol{B}_q, \qquad (3.12)$$

where the latter vector is often referred to as the Lipatov vertex.[2] In terms of these functions, the $N = 1$ opacity expression for the single gluon emission may be expressed as [25, 26]

$$\frac{-\boldsymbol{k}_S \cdot \boldsymbol{q}}{\boldsymbol{k}_S^2 (\boldsymbol{k}_S + \boldsymbol{q})^2} = \frac{1}{2} \left(\boldsymbol{L}_q^2 + \boldsymbol{A}_q^2 - \boldsymbol{B}_q^2 \right). \qquad (3.13)$$

We will refer back to this decomposition in section 4.

We now turn to the $C_F C_A^2$ contribution in the same limit. After expanding the prefactors and the phase factors in the manner described above, we find convenient to express the full answer in terms of the vectors

$$\boldsymbol{A}_g = \frac{\boldsymbol{\kappa}_S + \boldsymbol{q}}{(\boldsymbol{\kappa}_S + \boldsymbol{q})^2}, \quad \boldsymbol{B}_g = \frac{\boldsymbol{\kappa}_S}{\boldsymbol{\kappa}_S^2}, \quad \boldsymbol{L}_g = \boldsymbol{A}_g - \boldsymbol{B}_g, \qquad (3.14)$$

where $\boldsymbol{\kappa}_S$ has been defined in eq. (2.5). These functions are analogous to those of eq. (3.13) but, since they are functions of $\boldsymbol{\kappa}_S$ they may be viewed as the transverse momentum of the soft gluon as measured with respect to the hard one. In terms of these functions, the

---

[2]This vector is also known as the Gunion-Bertsch amplitude.

contribution to the cross section in which the hard gluon emits the soft one is given by

$$w_G(x^+; \boldsymbol{q}) = \frac{4g^2}{\boldsymbol{k}_H^2} \times 4g^4 \left\{ \left(\boldsymbol{L}_g^2 + \boldsymbol{A}_g^2 - \boldsymbol{B}_g^2 - \boldsymbol{A}_q \cdot \boldsymbol{L}_g\right) \left\{1 - \cos\left[\frac{(\boldsymbol{\kappa}_S + \boldsymbol{q})^2}{2k_S^+} x^+\right]\right\}\right.$$
$$- \boldsymbol{L}_q \cdot \boldsymbol{A}_g \left\{1 - \cos\left[\frac{(\boldsymbol{k}_S + \boldsymbol{q})^2}{2k_S^+} x^+\right]\right\}$$
$$+ \boldsymbol{L}_q \cdot \boldsymbol{L}_g \left\{1 - \cos\left[\left(\frac{(\boldsymbol{\kappa}_S + \boldsymbol{q})^2}{2k_S^+} - \frac{(\boldsymbol{k}_S + \boldsymbol{q})^2}{2k_S^+}\right) x^+\right]\right\}$$
$$\left. + \mathcal{C}\left(k_H^+, \boldsymbol{k}_H; k_S^+, \boldsymbol{k}_S\right) \sin\left[\frac{\boldsymbol{k}_S^2}{2k_S^+} x^+\right] \sin\left[\frac{\boldsymbol{q} \cdot \boldsymbol{k}_H}{k_H^+} x^+\right]\right\}, \quad (3.15)$$

where we have defined the function[3]

$$\mathcal{C}\left(k_H^+, \boldsymbol{k}_H; k_S^+, \boldsymbol{k}_S\right) = -\frac{1}{4} \frac{k_S^+}{k_H^+} \frac{\boldsymbol{\kappa}_S \cdot \boldsymbol{k}_H}{\boldsymbol{k}_H^2 \, \boldsymbol{k}_S^2 \, \boldsymbol{\kappa}_S^2} \quad (3.16)$$

Since $\mathcal{C}$ does not depend on $\boldsymbol{q}$, after integration over transferred momenta with the isotropic distribution $\mathcal{V}(\boldsymbol{q})$ in eq. (2.2), the last term of eq. (3.15) vanishes. Therefore, similarly to eq. (3.15), this contribution to the full rate is also proportional to the vacuum probability of emitting a hard gluon, $\sim 1/\boldsymbol{k}_H^2$. Combining eq. (3.11) and eq. (3.15) we may express the full answer for the double-inclusive gluon rate as

$$\langle|\mathcal{M}_{1\mathrm{OP}}|^2\rangle\Big|_{z\ll r} = \mathcal{P}_{\mathrm{vac}}\left(k_H\right) \times \mathcal{P}_{\mathrm{ant}}^{(1)}\left(k_S\right), \quad (3.17)$$

where $\mathcal{P}_{\mathrm{vac}}$ is the vacuum $q \to q + g$ splitting function in the soft limit

$$\mathcal{P}_{\mathrm{vac}}(k_H) = \frac{2C_F g^2}{k_H^2}, \quad (3.18)$$

and $\mathcal{P}_{\mathrm{ant}}^{(1)}$ is the emission rate of soft gluons off a hard quark-gluon dipole at first order in medium opacity, which we have derived in appendix B using the method of classical currents employed in [62]. $\mathcal{P}_{\mathrm{ant}}^{(1)}$ is given in eq. (B.15) and eq. (B.17), which we reproduce here for the readers convenience,

$$\mathcal{P}_{\mathrm{ant}}^{(1)} = 4g^4 C_A m_D^2 \int_{x^+} \int_{\boldsymbol{q}} n(x^+) \mathcal{V}(\boldsymbol{q})^2$$
$$\times \left\{ C_F(\boldsymbol{L}_q^2 + \boldsymbol{A}_q^2 - \boldsymbol{B}_q^2) \left\{1 - \cos\left[\frac{(\boldsymbol{k}_S + \boldsymbol{q})^2}{2k_S^+} x^+\right]\right\}\right.$$
$$+ C_A \left[(\boldsymbol{L}_g^2 + \boldsymbol{A}_g^2 - \boldsymbol{B}_g^2 - \boldsymbol{A}_q \cdot \boldsymbol{L}_g) \left\{1 - \cos\left[\frac{(\boldsymbol{\kappa}_S + \boldsymbol{q})^2}{2k_S^+} x^+\right]\right\}\right.$$
$$- \boldsymbol{L}_q \cdot \boldsymbol{A}_g \left\{1 - \cos\left[\frac{(\boldsymbol{k}_S + \boldsymbol{q})^2}{2k_S^+} x^+\right]\right\}$$
$$\left.\left. + \boldsymbol{L}_q \cdot \boldsymbol{L}_g \left\{1 - \cos\left[\left(\frac{(\boldsymbol{\kappa}_S + \boldsymbol{q})^2}{2k_S^+} - \frac{(\boldsymbol{k}_S + \boldsymbol{q})^2}{2k_S^+}\right) x^+\right]\right\}\right]\right\}, \quad (3.19)$$

---

[3]In spite of the explicit fraction k_S^+/k_H^+ in eq. (3.16), this term is of the same z-order as the rest of the terms in eq. (3.15).

which only depends on two dynamical time-scales,

$$\tau_q = \frac{2k_S^+}{(\boldsymbol{k}_S + \boldsymbol{q})^2}, \qquad \tau_g = \frac{2k_S^+}{(\boldsymbol{\kappa}_S + \boldsymbol{q})^2} \tag{3.20}$$

which are the formation times of the soft gluon when emitted collinear to the hard quark, τ_q, and to the hard gluon, τ_g.

The factorised form eq. (3.17) admits a simple physical interpretation of the emission rate. In this limit, in which the hard gluon cannot be medium-induced, its production is totally dominated by vacuum physics, and its rate is determined by the vacuum splitting function. Since, as shown in eq. (3.10), the formation time of the hard gluon is parametrically smaller than that of the soft gluon, the hard gluon is emitted early. From the point of view of the medium, the system behaves as a quark-gluon antenna right after the hard vertex. Therefore, the medium interacts with this two-parton systems simultaneously. The emission pattern includes several interferences effects, encoded in the intricate x^+ dependence of the rate, which are a result of the simultaneous propagation of this multi-parton system. We will discuss this pattern in detail in section 4.

3.3 Emission rate in the collinear limit

We now explore a different limit for the emission rate in which the hard gluon is not forced to be emitted first. To do so, we will consider the emission rate in the limit in which the ratio of angles goes to zero first ($r \to 0$) and then look for terms leading in the ratio of energies $z \ll 1$. The scaling of the momentum transferred with the transverse momentum of the medium gluon, eq. (3.7), implies that the order of limits does not commute, since, as expressed in eq. (3.8), in this limit the transverse momentum of the hard gluon, k_H, becomes parametrically smaller than q. The limit we performed may be summarised as,

$$r \to 0, \; z \to 0, \quad \text{with} \quad \{\tilde{q}, \theta_S, k_H^+\} \text{ fixed}. \tag{3.21}$$

It is easy to see from eq. (3.10) that in this limit the formation time of the hard gluon is parametrically longer than that of the soft emission.A sketch of this limit can be found in figure 5 right.

As before, we expand the pre-factors $\mathcal{P}_Q^{(i)}$ and $\mathcal{P}_G^{(i)}$ to leading order in r, which corresponds to r^{-2}. In this limit, only 1 out of the 2 terms in $\mathcal{P}_Q^{(i)}$ and 7 out of the 19 terms $\mathcal{P}_G^{(i)}$ are non-vanishing, and all of them depend on z as a power, z^{-2}. Unlike the previous case, not all the phase factors of the surviving terms possess the same leading r limit: 6 of the phase factors $\tau_G^{(i)}$ are $\mathcal{O}(r^0)$ and the remaining one is $\mathcal{O}(r^2)$. The presence of the additional scale x^+ allows us to keep the latter apparently suppressed time-scale, which becomes important at times of order r^{-2}. Nevertheless, in the leading r limit, all 6 terms with $\mathcal{O}(r^0)$ phases cancel identically, leading to

$$w_Q(x^+; \boldsymbol{q}) = \frac{4g^2}{\boldsymbol{k}_H^2} \times (-8g^4) \frac{\boldsymbol{k}_S \cdot \boldsymbol{q}}{\boldsymbol{k}_S^2 (\boldsymbol{k}_S + \boldsymbol{q})^2} \left\{ 1 - \cos \left[\frac{(\boldsymbol{k}_S + \boldsymbol{q})^2}{2k_S^+} x^+ \right] \right\}, \tag{3.22}$$

$$w_G(x^+; \boldsymbol{q}) = \frac{4g^2}{\boldsymbol{k}_H^2} \times 4g^2 \frac{q^2}{\boldsymbol{k}_S^2 (\boldsymbol{k}_S + \boldsymbol{q})^2} \left\{ 1 - \cos \left[\frac{\boldsymbol{k}_H^2}{2 k_H^+} x^+ \right] \right\}. \tag{3.23}$$

As in the previous limit, both terms of the emission amplitude are proportional to $\mathcal{P}_{\text{vac}}$, eq. (3.18), which implies that the production of the hard gluon proceeds as in vacuum. This is a consequence of the fact that in this limit k_H is parametrically smaller than q. Due to LPM interference, the medium-induced rate is collinear finite [25, 26], implying that gluons with $k_H \ll q$ cannot be medium-induced and, therefore, have to have been generated in the hard vertex that creates the jet.

The soft gluon emission rate depends on two distinct time-scales. The emission rate of soft gluons off the quark, $w_Q(x^+; \boldsymbol{q})$, is identical in both limits, eq. (3.11) and eq. (3.22), which, as we have discussed coincides with the $N = 1$ opacity spectrum. This spectrum is controlled by the formation time of the soft gluon in medium τ_q. The contribution to the rate coming from emissions off the hard gluon, $w_G(x^+; \boldsymbol{q})$, is different in this limit. This rate no longer depends on the time-scale τ_g, as eq. (3.15). The time-scale controlling interferences in eq. (3.23) is the formation time of the hard gluon, $\tau_H = 2k_H^+/\boldsymbol{k}_H^2$.

The appearance of τ_H in the emission rate leads to a simple consequence. If the medium interacts with the quark-gluon system prior to the formation of the hard gluon, $x^+ \ll \tau_H$, the emission rate is dominated by radiation off the quark, since the eq. (3.23) vanishes. After τ_H, the emission rate may be understood as the incoherent superposition of the radiation off the quark plus the radiation off the gluon. At these late times, the rate of emission off the hard gluon is given by the Gunion-Bertsch term [79],

$$\lim_{r \to 0} \boldsymbol{L}_g^2 = \frac{\boldsymbol{q}^2}{\boldsymbol{k}_S^2 \, (\boldsymbol{k}_S + \boldsymbol{q})^2} \,, \tag{3.24}$$

where $\boldsymbol{L}_g$ is defined in eq. (3.14), which corresponds to the emission of a soft gluon of momentum $\boldsymbol{k}_S$ off a hard on-shell gluon generated infinitely far away from the scattering centre. This rate differs from the emission rate of the soft gluon off the quark, eq. (3.22), which is the $N = 1$ spectrum.

This difference in the emission rate implies that after the formation of the gluon, this new source of colour does not radiate in-medium as an independent new source produced at τ_H, which would lead to an equivalent $N = 1$ spectrum off the hard gluon. The origin of the different rates at asymptotic late times may be understood from the analysis of the antenna spectrum, eq. (3.19). First of all, we note that in the limit eq. (3.21), the time-scales that control the emission from the colour dipole are parametrically suppressed with respect to τ_H. In the small r limit

$$\frac{\tau_H}{\tau_q} = \mathcal{O}\left(\frac{z}{r^2}\right) \,, \quad \frac{\tau_H}{\tau_g} = \mathcal{O}\left(\frac{z}{r^2}\right) \,, \quad \frac{\tau_H}{\tau_q} - \frac{\tau_H}{\tau_g} = \mathcal{O}\left(\frac{z}{r}\right) \,. \tag{3.25}$$

Because of this separation of time-scales, the relevant limit of the antenna spectrum eq. (3.19) is to consider $x^+ \to \infty$, which implies that all phase factors average out to zero. In this incoherent limit, together with eq. (3.21), the part of the antenna spectrum proportional to C_A is

$$\lim_{r \to 0} \left(\boldsymbol{L}_g^2 + \left(\boldsymbol{A}_g^2 - \boldsymbol{A}_q \cdot \boldsymbol{A}_g \right) - \left(\boldsymbol{B}_g^2 - \boldsymbol{B}_q \cdot \boldsymbol{B}_g \right) \right) = \frac{\boldsymbol{q}^2}{\boldsymbol{k}_S^2 \, (\boldsymbol{k}_S + \boldsymbol{q})^2} \,, \tag{3.26}$$

which coincides with the Gunion-Bertsch rate found in the two-gluon cross section.

This observation leads to a simple interpretation of the full double emission rate. If the medium exchange is placed early compared to τ_H, the interaction of the vacuum jet with the medium is identical to the interaction of a hard quark with the medium; the emission of the hard gluon occurs after the scattering, and proceeds as in vacuum. If, on the contrary, the interaction with the medium occurs at a time long compared to τ_H, then the hard gluon has time to form via vacuum processes, leading to the generation of an in-medium antenna. From this time on, it is the quark-gluon dipole the one that interacts with the medium. We will discuss the consequences of this interpretation in section 4.

4   Discussion and outlook

In this paper we have discussed two particular kinematic regions, summarised in eq. (3.9) and eq. (3.21), of the emission rate of two gluons in a thin (opacity $N = 1$) medium. These limits are particularly interesting because they allow us to cleanly separate vacuum and medium emissions. As we have discussed, in both those kinematic regions the emission of one of the gluons, the hard gluon, is dominated by vacuum-like processes produced at the hard vertex that creates a jet, while the soft gluon is medium-induced.[4] By choosing these kinematics, we have focused on understanding how the multi-parton state associated to the propagation of a jet in plasma interacts with a QCD medium. However, this limit prevents us from studying how the emission of new partons by medium-induced processes interferes with the evolution of the jet shower, which demands the analysis of the rate when both emitted gluons can be medium-induced. This is a more intricate analysis which we leave for future work. Other analyses of the rate of emission of two gluons of comparable momentum from an on-shell quark propagating in the plasma can be found in [56, 57].

As we have shown, within these regions the emission pattern of soft gluons is controlled by the emission spectrum off a hard quark-gluon dipole in medium, eq. (3.19). This type of dipoles has been recently used to understand emissions by multiple colour sources in plasma and led to a rich interference structure [58–63]. The particular case of opacity $N = 1$ for a colour singlet antenna was analysed in detail in [62]. Although the main lessons of the interference emission pattern of the quark-gluon antenna may be inferred from the analysis of the colour singlet antenna in [62], for completeness we discuss those features below.

The antenna emission rate is controlled by three distinct time-scales: the in-medium formation times of soft gluons emitted off the quark, τ_q, and off the gluon, τ_g, defined in eq. (3.20) and a third time-scale, intrinsically multi-partonic, which combines kinematic information of both constituents of the antenna,

$$\tau_{\rm res}^{-1} = \frac{1}{\tau_q} - \frac{1}{\tau_g} = \frac{2\boldsymbol{q} - \boldsymbol{k}_S - \boldsymbol{\kappa}_S}{2}\,\mathbf{n}, \qquad (4.1)$$

with $\mathbf{n} = \boldsymbol{k}_H/k_H^+$ a vector in transverse space whose modulus is the opening angle of the quark-gluon system, $\mathbf{n}^2 = \theta_H^2$. This time-scale controls the interference between medium-induced emissions of the two sources.

---

[4]Note that the two gluon emission rate we have computed is, overall, medium induced, since it is estimulated by a medium exchange. Nevertheless, this rate can be understood as a combination of vacuum-like processes and medium-induced single emissions processes.

To understand how these interferences occur, let us first consider the induced spectrum off the quark-gulon dipole when the angle of the antenna θ_H is large. In this limit, the stimulated emissions off the quark and off the hard gluon are independent of one another. The medium-induced spectrum off each of the propagating sources is dominated by gluons emitted with a typical transverse momentum *with respect to the source* of order m_D; this means that medium-induced gluons off the quark have $k_S \sim m_D$ while the induced gluons off the hard gluon have $\kappa_S \sim m_D$. Therefore, the induced spectrums will be well separated from one another if the angle of the dipole $\theta_H \gg \theta_{\text{med}}$, with $\theta_{\text{med}} = m_D/k_S^+$ being the typical emission angle with respect to the emitting source. In this limit, as a consequence of eq. (3.5), medium-induced gluons off the quark have $\kappa_S \approx k_S^+ \theta_H \gg k_S$ and induced gluons off the hard gluon have $k_S \approx k_S^+ \theta_H \gg \kappa_S$. This condition is sufficient to show that, up to corrections of order $\theta_{\text{med}}^2/\theta_H^2$, the antenna spectrum eq. (3.19), is the incoherent superposition of the stimulated spectrum off the quark and off the hard gluon.

Complementary, soft gluon emission off the antenna suffers from strong interferences for $\theta_H \ll \theta_{\text{med}}$. In this limit, for typical induced gluons $\kappa_S \approx k_S \sim m_D$, which implies that $\tau_q \approx \tau_g$, $\boldsymbol{A}_q \approx \boldsymbol{A}_g$, $\boldsymbol{B}_q \approx \boldsymbol{B}_g$ and $\boldsymbol{L}_q \approx \boldsymbol{L}_g$. The antenna spectrum is reduced to

$$w_{\text{ant}}^{(1)}\left(x^+; \boldsymbol{k}_S, k_S^+\right)\Big|_{\theta_H \ll \theta_{\text{med}}} = C_F \left[1 - \cos\frac{x^+}{\tau_q}\right] \left(\boldsymbol{L}_q^2 + \boldsymbol{A}_q^2 - \boldsymbol{B}_q^2\right) + C_A \left[1 - \cos\frac{x^+}{\tau_{\text{res}}}\right] \boldsymbol{L}_q^2, \tag{4.2}$$

which is the medium-induced spectrum off the quark plus an additional interference term encoding the emission off the gluon. In the small dipole limit, for typical induced gluons eq. (4.1) yields $\tau_{\text{res}}^{-1} \sim m_D \theta_H$. Therefore, interferences between the two sources suppress the emission off the hard gluon if at the relevant observation time x^+ the transverse size of the dipole is $\lambda = \theta_H x^+ \ll \lambda_{\text{res}}$, with

$$\lambda_{\text{res}} = \frac{1}{m_D} \tag{4.3}$$

the *transverse resolution scale*, which in this dilute medium equals the inverse typical momentum transferred by the medium.

The characteristic time-scale for medium-induced radiation is the formation time of the emitted gluon, τ_q. At this time, the typical transverse size of the quark-gluon dipole is $\lambda \sim \lambda_{\text{res}} \theta_H/\theta_{\text{res}}$. Therefore, for induced gluons with $\theta_{\text{res}} \gg \theta_H$ the transverse size of the dipole at emission is small compared to the transverse resolution scale and the spectrum is totally dominated by the emission off the hard quark. Nevertheless, the condition $\theta_{\text{res}} \gg \theta_H$ depends on the frequency of the soft gluon, and at fixed θ_H only a fraction of the induced spectrum, with $k_S^+ \ll m_D/\theta_H$, is suppressed by interference effects. Since LPM interference suppresses induced radiation with formation time larger than the medium length L, the medium-induced spectrum has a maximum frequency of emission, $\omega_{\text{max}} \sim m_D^2 L$ [25–27]. Therefore, if the dipole opening angle $\theta_H \ll 1/m_D L$, all the medium-induced spectrum off the gluon is cancelled by interference, and the full emission spectrum off the quark-gluon dipole is given by the medium-induced radiation off a hard quark. The multipartonic system interacts with the plasma as a single colour charge, the total charge of the system, as long as its maximal transverse size in the medium $\theta_H L \ll \lambda_{\text{res}}$. As we have seen, the rich

interference structure associated to the medium resolution scale λ_{res} emerges in the soft limit of the double gluon emission rate, eq. (3.17), in which the emission of a hard gluon may be viewed as the production of an in-medium antenna.

The emergence of the antenna interference pattern suggests a simple organising principle to understand the dynamics of jet showers in medium based on the resolution scale, as already suggested in [65]. A basic element of this picture is that, similarly to vacuum, jet showers may be best understood as a collection of in-medium antennas, that are dynamically generated in the process of relaxation of the virtuality of the jet. Our computations in the small angle regime support this picture. As we have seen in section 3.3, the emission of soft gluons by a quark-gluon system generated in vacuum explicitly depends on the formation time of the gluon τ_H. While for short times $x^+ \ll \tau_H$ the emission pattern off the quark-gluon system is just that off a quark, after τ_H both the quark and the hard gluon contribute to the emission spectrum. This agrees with the common approximation of considering τ_H as the time in which the hard gluon decorrelates from the hard quark. Nevertheless, disregarding the trivial differences in colour factors, the emission spectrums of the quark and gluon are not identical. Therefore, a naive iteration of the medium-induced spectrum after the formation of the hard gluon leads to the incorrect emission rate.

As we have shown, the emission rate off the hard gluon is predicted from the antenna picture in the small angle limit, provided the antenna forms after τ_H. The physical origin of the discrepancy between the iteration of the $N = 1$ opacity spectrum, eq. (3.22), and the antenna prediction is easy to understand. As it is well known, in the totally incoherent limit ($\tau_q \ll x^+$) the emission rate can be expressed as eq. (3.13), which we reproduce here for convenience,

$$\frac{-2\,\boldsymbol{k}_S \cdot \boldsymbol{q}}{(\boldsymbol{k}_S + \boldsymbol{q})^2 \boldsymbol{k}_S{}^2} = \boldsymbol{L}_q^2 + \boldsymbol{A}_q^2 - \boldsymbol{B}_q^2, \tag{4.4}$$

which shows that the emission rate is the sum of the stimulated emission off an on-shell quark, $\boldsymbol{L}_q^2$, the medium broadening of a soft gluon produced in the hard vertex, $\boldsymbol{A}_q^2$, and a unitarity correction which subtracts strength from the vacuum emission rate of soft gluons off the quark, $\boldsymbol{B}_q^2$. The difference in the in-medium rate off the hard gluon lies precisely in a different *vacuum* emission rate of soft gluons by the quark-gluon antenna. As shown in eq. (B.12), because of the interference with the quark, the vacuum emission of soft gluons off the hard gluon is proportional to

$$\mathcal{P}_{\text{vac}}^G \propto (\boldsymbol{B}_g - \boldsymbol{B}_q)^2 \ , \tag{4.5}$$

where the dependence in $\boldsymbol{B}_q$ reflects the interference with the quark. This vacuum rate vanishes in the limit of $\theta_H \ll \theta_S$, since, on the formation time of the vacuum soft gluon, the transverse size of the quark-gluon dipole is negligible. This does not imply that the in-medium rate vanishes, since, in the limit eq. (3.21), $\tau_H \sim 1/k_H^+ \theta_S r^2$ and the dipole has a (parametrically) long time to separate, leading to a large transverse separation at formation time $\Delta = \theta_H \tau_H \sim z/r k_S$. As a result of vacuum interference, the emission off the gluon coincides with the emission off an on-shell gluon generated infinitely far away from the medium, since no soft gluons are produced in vacuum in this kinematic lint.

The small angle approximation explored in section 3.3 is, however, insensitive to the the medium resolution scale $\lambda_{\rm res}$. For typical in medium radiation with $k_S \sim m_D$, at the time the hard gluon forms the transverse size of the dipole is $\lambda = \lambda_{\rm res} z/r \gg \lambda_{\rm res}$ and the antenna is totally resolved. For this reason, at times long compared to τ_H the two gluon emission rate, eq. (3.22) and eq. (3.23), coincides with the spectrum of a fully resolved $(x^+ \to 0)$ small angle antenna, eq. (4.2). Unfortunately, the limit in which $r \to 0$ first is inadequate to explore the interplay between $\lambda_{\rm res}$ and the formation of the hard gluon. In future work we plan to address the limit $r \sim z \to 0$ to understand how the formation of the antenna affects the resolution of the colour structure of the propagating dipole.

Acknowledgments

A Effective Feynman rules in the eikonal limit

Here we will shortly review the relevant Feynman diagram technique applied in the light-cone gauge in the mixed representation, which is quite similar to the so-called time-ordered perturbation theory. Choosing the gauge vector to be purely "minus", $n \equiv (0, 1, \mathbf{0})$, leads to the gauge condition $n \cdot A = A^+ = 0$ for the gluon field. In particular, the gluon polarization vector becomes

$$\varepsilon_\lambda(k) = \left(0, \frac{\mathbf{k} \cdot \boldsymbol{\varepsilon}_\lambda(\mathbf{k})}{k^+}, \boldsymbol{\varepsilon}_\lambda(\mathbf{k})\right). \tag{A.1}$$

A.1 Propagators

The scalar (Feynman) propagator for massless particles in vacuum reads

$$D(k) = \frac{i}{k^2 + i\epsilon}, \tag{A.2}$$

In terms of this, the quark and gluon propagators read

$$S(k) = \sum_s u^s(k)\bar{u}^s(k) D(k), \tag{A.3}$$

$$G^{\mu\nu}(k) = \sum_\lambda \varepsilon_\lambda^{*\,\mu}(k)\varepsilon_\lambda^\nu(k) D(k), \tag{A.4}$$

respectively, where

$$\sum_s u^s(k)\bar{u}^s(k) = \not{k}\,, \tag{A.5}$$

$$\sum_\lambda \varepsilon^{*\,\mu}(k)\varepsilon^\nu(k) = -g^{\mu\nu} + \frac{k^\mu n^\nu + k^\nu n^\mu}{k \cdot n} - k^2 \frac{n^\mu n^\nu}{(k \cdot n)^2}\,. \tag{A.6}$$

The transverse part of the polarization vectors satisfy $\sum_\lambda \varepsilon_\lambda^{*\,i}\varepsilon_\lambda^j = \delta^{ij}$. Since all propagating partons are put on-shell, the latter term in eq. (A.6) is irrelevant for our analysis. The gluon propagator is symmetric, and the only non-vanishing components read

$$G^{--}(k) = \frac{\boldsymbol{k}^2}{(k^+)^2}D(k)\,, \quad G^{-i}(k) = \frac{k^i}{k^+}D(k)\,, \quad G^{ij}(k) = \delta^{ij}D(k)\,, \tag{A.7}$$

where $i = (1, 2)$. In the next subsection we will show that in the eikonal limit all the vertices become transverse and diagonal in spin and polarization, which allows them to absorb all the quark/gluon dependence (numerators). This leaves us with the momentum flow and pole structure which are encoded exlusively in the scalar part of the propagator.

We will work in the mixed representation, with (light-cone) time, energy and transverse momentum. For instance, energy-momentum conservation in a $q(l) \to q(p) + g(k)$ takes the following form

$$(2\pi)^4\delta^{(4)}(p + k - l) = (2\pi)^3 \int \mathrm{d}x^+\, e^{i(p^- + k^- - l^-)x^+}\, \delta\left(p^+ + k^+ - l^+\right) \delta\left(\boldsymbol{p} + \boldsymbol{k} - \boldsymbol{l}\right)\,, \tag{A.8}$$

and similarly for the four-gluon vertex. While external particles are naturally required to be on-shell, the mixed representation also allows to put all internal propagators on-shell, by

$$D(x^+; k) \equiv D(x^+; \boldsymbol{k}, k^+) = \int_{-\infty}^{\infty} \frac{\mathrm{d}k^-}{2\pi} e^{-ik^-x^+}\, D(k)\,, \tag{A.9}$$

$$= \frac{\Theta(x^+)}{2k^+} e^{-ik^-x^+ - \epsilon x^+}\,, \tag{A.10}$$

with $k^- = \boldsymbol{k}^2/(2k^+)$ in the last line. The ϵ-prescription regulates the behavior of the propagator at infinity. We note that we have to keep in mind that any integration of an *external* point involves the additional phases as in eq. (A.8).

A.2 Leading eikonal vertices

Here we derive the relevant vertices and demonstrate their behavior in the eikonal approximation. This means that we only keep terms that are enhanced by a factor z^{-1}, where z is the fraction of a small energy over a large one. This automatically leads to the preservation of (quark) helicity and (gluon) polarization that floats through the vertices.

The triple gluon vertex reads

$$iV_{abc}^{\mu\nu\sigma}(K_1, K_2, K_3) = gf^{abc}\left[(K_1 - K_2)^\sigma g^{\mu\nu} + (K_2 - K_3)^\mu g^{\nu\sigma} + (K_3 - K_1)^\nu g^{\mu\sigma}\right]\,, \tag{A.11}$$

where all momenta are incoming and f^{abc} is the SU(3) structure constant. Enforcing energy-momentum conservation in the vertex, we will define the emission vertex describing $g(K_1 + K_2) \to g(K_1) + g(K_2)$, where the momentum flow follows the time flow, as

$$\Gamma_G^{abc}(K_1, K_2) = \varepsilon_\mu^*(K_1)\varepsilon_\sigma^*(K_2)\, iV_{abc}^{\mu\nu\sigma}(-K_1, K_1 + K_2, -K_2)\, \varepsilon_\nu(K_1 + K_2)$$

$$= 2gf^{abc}\left[\frac{1}{z}\left(\boldsymbol{\kappa} \cdot \boldsymbol{\varepsilon}_2\right)\left(\boldsymbol{\varepsilon}_2 \cdot \boldsymbol{\varepsilon}_{12}\right) + \left(\boldsymbol{\kappa} \cdot \boldsymbol{\varepsilon}_1\right)\left(\boldsymbol{\varepsilon}_2 \cdot \boldsymbol{\varepsilon}_{12}\right) - \frac{1}{1+z}\left(\boldsymbol{\kappa} \cdot \boldsymbol{\varepsilon}_{12}\right)\left(\boldsymbol{\varepsilon}_1 \cdot \boldsymbol{\varepsilon}_2\right)\right],$$
(A.12)

where $\boldsymbol{\kappa} \equiv \boldsymbol{k}_2 - z\boldsymbol{k}_1$, $z \equiv k_2^+/k_1^+$ and $\boldsymbol{\varepsilon}_i \equiv \boldsymbol{\varepsilon}(\boldsymbol{k}_i)$. In the eikonal approximation we only keep the leading z term in eq. (A.12). We will however keep the apparently sub-leading contribution to $\boldsymbol{\kappa}$ since $|\boldsymbol{\kappa}| \sim k^+(\theta_1 + \theta_2)$ and we are interested in arbitrary angular ordering. The eikonal triple-gluon vertex becomes completely transverse and reads

$$\Gamma_G^{abc,k}(\boldsymbol{k}_1, k_1^+; \boldsymbol{k}_2, k_2^+) = 2gf^{abc}\frac{1}{z}\kappa^k,$$
(A.13)

where we have dropped a diagonal matrix for the propagation of the polarization. This ensures that the polarization of the hardest gluon is conserved in the vertex. On the other hand, including one gluon field from the medium in the triple gluon vertex leads to

$$\varepsilon_\mu^*(K_1)A_\sigma^c(K_2)\, iV_{abc}^{\mu\nu\sigma}(-K_1, K_1 - K_2, K_2)\, \varepsilon_\nu(K_1 - K_2)$$
$$= 2gf^{abc}k_1^+ A^{c-}(K_2)\, \boldsymbol{\varepsilon}_1 \cdot \boldsymbol{\varepsilon}_{12}.$$
(A.14)

Using the decomposition in eq. (2.1) for the medium potential and applying the transformation to the mixed representation allows us to define a triple-gluon interaction vertex

$$U_G^{ab}(x^+; k^+, \boldsymbol{q}) = 2g\, k^+\, f^{abc}\mathcal{A}^c(x^+, \boldsymbol{q}),$$
(A.15)

$$= u_G^{abc}(k^+)\, \mathcal{A}^c(x^+, \boldsymbol{q}),$$
(A.16)

where the transversality of the vertex is again suppressed.

Following the same approach as for the gluons, we will define properly contracted QCD vertices that absorb the numerators of the propagators. For the emission of a gluon, $q(K_1 + K_2) \to q(K_1) + g(K_2)$, we define

$$V_G(K_1, K_2) = \bar{u}^t(K_1)\big(ig\gamma^\mu t^a\big)\varepsilon_\lambda^{*\,\mu}(K_2)\, u^s(K_1 + K_2),$$
(A.17)

where t^a is the SU(3) generator in the fundamental representation. In the eikonal limit, we take advantage of $\bar{u}^t(K_1)\gamma^\mu u^s(K_1 + K_2) = 2K_1^\mu \delta^{ts} + \mathcal{O}(K_2/K_1)$, which conserves spin, to define

$$V_G^{a,i}(\boldsymbol{k}_1, k_1^+; \boldsymbol{k}_2, k_2^+) = 2ig\, t^a \frac{1}{z}\kappa^i,$$
(A.18)

where again $\boldsymbol{\kappa} \equiv \boldsymbol{k}_2 - z\boldsymbol{k}_1$ and $z \equiv k_2^+/k_2^+$ and we have suppressed a diagonal matrix for the spin components. For the interaction with the medium we simply replace the polarization vector $\varepsilon_\lambda^{*\,\mu}(K_2)$ in eq. (A.17) by the medium field $A^\mu(Q)$, and find

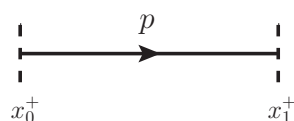$$U_Q(x^+; k^+, \boldsymbol{q}) = 2ig\, k^+\, t^a \mathcal{A}^a(x^+, \boldsymbol{q}),$$
(A.19)

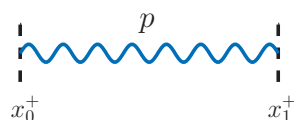$$= u_Q^a(k^+)\, \mathcal{A}^a(x^+, \boldsymbol{q}).$$
(A.20)

We note that the newly defined emission vertices, eq. (A.13) and eq. (A.18), allow us to absorb all spin and polarization information contained in the numerator of the quark and gluon propagators. We are therefore left with scalar propagators and the vertices for emission and interaction. The interaction vertices, eq. (A.15) and eq. (A.19), are scalars as well.
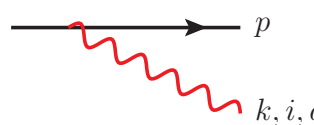
A.3 Effective Feynman rules

As a summary, we provide a list of graphical rules that can be used in order to calculate any diagram in light-cone perturbation theory in the mixed representation.
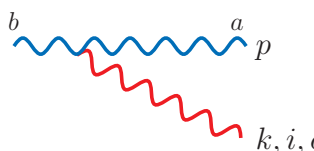
$$= D\left(x_1^+ - x_0^+; p^+, \boldsymbol{p}\right), \tag{A.21}$$
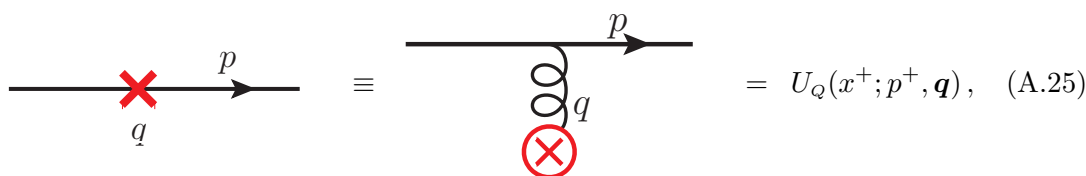
$$= D\left(x_1^+ - x_0^+; p^+, \boldsymbol{p}\right), \tag{A.22}$$
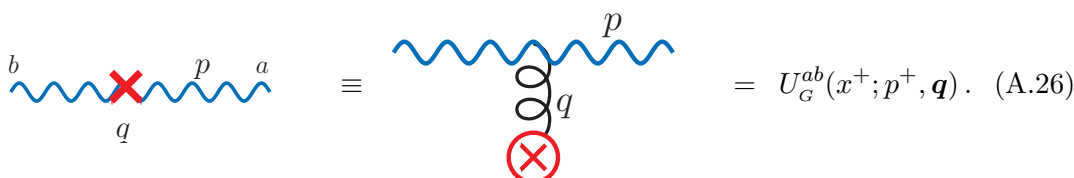

$$= V_G^{a,i}(\boldsymbol{\kappa}, z), \tag{A.23}$$

$$= \Gamma_G^{abc,i}(\boldsymbol{\kappa}, z), \tag{A.24}$$

$$= U_Q(x^+; p^+, \boldsymbol{q}), \tag{A.25}$$

$$= U_G^{ab}(x^+; p^+, \boldsymbol{q}). \tag{A.26}$$

Finally, we will discuss the situation where the same parton line interacts twice with the medium. Due to the instantaneous nature of the interactions, see eq. (2.2), the scalar propagator in between the two medium-insertions reduces to $\Theta(0)/(2k^+) = 1/(4k^+)$ and the double-interaction is denoted by a circle instead of two crosses. Since we can perform

the integrations over the medium-momentum explicitly, we obtain the following two rules

 $\qquad = -\dfrac{1}{2}\alpha_s C_F \displaystyle\int \mathrm{d}x^+\, n(x^+)\,,$ (A.27)

 $\qquad = \dfrac{1}{2}\alpha_s C_A \displaystyle\int \mathrm{d}x^+\, n(x^+)\,,$ (A.28)

where, in order to obtain explicit expressions, we have assumed that $\mathcal{V}(\boldsymbol{q}) = (\boldsymbol{q}^2 + m_D^2)^{-2}$. However, in our Mathematica code we have calculated these diagrams using the automated procedure similarly to all the other diagrams.

Additionally, all newly produced final-state partons, i.e., partons that propagate from some vertex to the cut, have to be multiplied by the appropriate polarization vector, for gluons, or spinor, for fermions, and by the appropriate phase $e^{ip^-x^+}$, where p is the parton momentum and x^+ the position of the last vertex. We summarise these rules below:

$$\text{} \qquad = e^{-ip^-x^+} u^s(p)\,, \tag{A.29}$$

$$\text{} \qquad = e^{-ip^-x^+} \bar{u}^s(p)\,, \tag{A.30}$$

$$\text{} \qquad = e^{-ip^-x^+} \varepsilon_\lambda^i(p)\,, \tag{A.31}$$

and similarly for final-state particles,

$$\text{} \qquad = e^{ip^-x^+} \bar{u}^s(p)\,, \tag{A.32}$$

$$\text{} \qquad = e^{ip^-x^+} u^s(p)\,, \tag{A.33}$$

$$\text{} \qquad = e^{ip^-x^+} \varepsilon_\lambda^{*\,i}(p)\,, \tag{A.34}$$

where the "cut" (corresponding to $x^+ = \pm\infty$) is represented by a small vertical line.

B   Short derivation of the antenna spectrum in medium

Since soft gluon radiation can be treated as a classical process, we can apply methods from classical Yang-Mills theory to obtain the amplitude for an emission off one of the legs of the antenna, which reads

$$
\mathcal{M}^a_{\lambda,1} = 2ig \int_{\boldsymbol{q}} \int_0^\infty \mathrm{d}x^+ \left[T \cdot \mathcal{A}(x^+; \boldsymbol{q}) \right]^{ab} \tilde{q}_1^b
$$
$$
\times \left\{ \frac{\boldsymbol{\kappa}_1 - \boldsymbol{q}}{(\boldsymbol{\kappa}_1 - \boldsymbol{q})^2} - \left[\frac{\boldsymbol{\kappa}_1 - \boldsymbol{q}}{(\boldsymbol{\kappa}_1 - \boldsymbol{q})^2} - \frac{\boldsymbol{\kappa}_1}{\boldsymbol{\kappa}_1^2} \right] e^{i\frac{(\boldsymbol{\kappa}_1 - \boldsymbol{q})^2}{2k^+}x^+} \right\} \cdot \boldsymbol{\varepsilon}_\lambda(\boldsymbol{k}), \tag{B.1}
$$

where

$$
\boldsymbol{\kappa}_1 = \boldsymbol{k} - \frac{k^+}{p_1^+}\boldsymbol{p}_1, \tag{B.2}
$$

is the transverse momentum of the gluon $\boldsymbol{k}$ with respect to the transverse momentum of one of the legs of the antenna and $[T \cdot \mathcal{A}]^{ab}\tilde{q}_1^b = if^{abc}\mathcal{A}^b\tilde{q}_1^c$. The full amplitude, corresponding to emissions off both legs reads simply $\mathcal{M}^a_{\lambda,1+2} = \mathcal{M}^a_{\lambda,1} + \mathcal{M}^a_{\lambda,2}$. The inclusive one-gluon cross section reads then

$$
\frac{\mathrm{d}N}{\mathrm{d}^3k} = \frac{1}{(2\pi^3)2k^+} \sum_{\lambda,\lambda',a,a'} \langle \mathcal{M}^a_{\lambda,1+2} \mathcal{M}^{*,a'}_{\lambda',1+2} \rangle, \tag{B.3}
$$

where the brackets $\langle \ldots \rangle$ imply the medium average defined in eq. (2.2). The medium-induced spectrum is obtained from this after redifining the potential as

$$
\mathcal{V}(\boldsymbol{q}) \rightarrow \mathcal{V}(\boldsymbol{q}) - (2\pi)^2 \delta(\boldsymbol{q}) \int_{\boldsymbol{q}'} \mathcal{V}(\boldsymbol{q}'), \tag{B.4}
$$

in order to account for virtual corrections in a completely analogous way to the medium-virtual diagrams considered in the Feynman diagram technique utilized in the remainder of the paper.

A very similar situation to the one we are considering in the current work is the emission of a soft gluon off a colour dipole, or usually called an "antenna". We will label each of the emitters in this case simply by "1" and "2", and their kinematics is given by $p_i = (p_i^+, p_i^-, \boldsymbol{p}_i)$ while the momentum of the emitted gluon is $k = (k^+, k^-, \boldsymbol{k})$. Using the results in [62], we will here generalise their results for an antenna in a general colour configuration.

In vacuum, the square of the emission amplitude summed over colours and polarizations reads

$$
\mathcal{P}^{(0)}_{\mathrm{ant}}(k) \equiv \sum_\lambda \left| \mathcal{M}^{(0)}_\lambda \right|^2 = 4g^2 \left(\tilde{q}_1^2 \frac{1}{\boldsymbol{\kappa}_1^2} + \tilde{q}_2^2 \frac{1}{\boldsymbol{\kappa}_2^2} + 2\tilde{q}_1 \cdot \tilde{q}_2 \frac{\boldsymbol{\kappa}_1 \cdot \boldsymbol{\kappa}_2}{\boldsymbol{\kappa}_1^2 \boldsymbol{\kappa}_2^2} \right), \tag{B.5}
$$

where

$$
\boldsymbol{\kappa}_i \equiv \boldsymbol{k} - z_i \boldsymbol{p}_i, \tag{B.6}
$$

with $z_i \equiv k^+/p_i^+$ is the light-cone momentum fraction, is the transverse momentum of the emitted gluon with respect to the emitting antenna constituent.

In order to simplify the colour algebra, we have introduced the colour vectors $\mathcal{Q}_1^a$ and $\mathcal{Q}_2^a$ that obey the property $\mathcal{Q}_1^a + \mathcal{Q}_2^a = \mathcal{Q}_3^a$, where $\mathcal{Q}_3^2 \equiv \mathcal{Q}_3^a \cdot \mathcal{Q}_3^a$ is the total charge of the antenna. These vectors are defined such that for a quark $\mathcal{Q}_q^2 = C_F$, while for a gluon $\mathcal{Q}_g^2 = C_A$, where $C_F = (N_c^2 - 1)/(2N_c)$ and $C_A = N_c$. Finally, by squaring this relation we solve for the cross-term to find $\mathcal{Q}_1 \cdot \mathcal{Q}_2 = (\mathcal{Q}_3^2 - \mathcal{Q}_1^2 - \mathcal{Q}_2^2)/2$. The possible QCD $1 \to 2$ splittings give

$$\mathcal{Q}_1^2 = \mathcal{Q}_2^2 = C_F, \text{ and } \mathcal{Q}_3^2 = C_A \quad \text{for } g \to q + \bar{q}\,, \tag{B.7}$$

$$\mathcal{Q}_1^2 = \mathcal{Q}_2^2 = \mathcal{Q}_3^2 = C_A \quad \text{for } g \to g + g\,, \tag{B.8}$$

$$\mathcal{Q}_1^2 = \mathcal{Q}_3^2 = C_F, \text{ and } \mathcal{Q}_2^2 = C_A \quad \text{for } q \to q + g\,. \tag{B.9}$$

While the first two situations were analysed in references [58–63], we are mostly interested in the latter process for the moment. Let us also introduce a compact notation that will prove very useful in the following sections. First, we define the building blocks

$$\boldsymbol{A}_1^a \equiv \mathcal{Q}_1^a \frac{\boldsymbol{\kappa}_1 - \boldsymbol{q}}{(\boldsymbol{\kappa}_1 - \boldsymbol{q})^2}\,, \tag{B.10}$$

$$\boldsymbol{B}_1^a \equiv \mathcal{Q}_1^a \frac{\boldsymbol{\kappa}_1}{\boldsymbol{\kappa}_1^2}\,, \tag{B.11}$$

where the former will come in handy for the medium part. Note that $\boldsymbol{A}^a$ and $\boldsymbol{B}^a$ are both transverse vectors and vectors in colour space; dropping the superscript "a" simply defines the corresponding transverse vector. The same goes for any other similarly defined vector below.

For the colour configuration (B.9), the vacuum emission antenna spectrum takes the form

$$\mathcal{P}_{\text{ant}}^{(0)}(k) = 4g^2 \left[C_F \boldsymbol{B}_1^2 + C_A \left(\boldsymbol{B}_2^2 - \boldsymbol{B}_1 \cdot \boldsymbol{B}_2 \right) \right]\,. \tag{B.12}$$

Due to the colour algebra, the antenna quark radiates as a free one. This comes about due to the combination of the radiation inside the cone off the antenna legs and the large-angle radiation outside the cone by the total charge. Additionally, the gluonic antenna leg can radiate inside the cone.

Proceeding now to the situation where one medium interaction is allowed, we define the currents

$$\boldsymbol{L}_1^a \equiv \boldsymbol{A}_1^a - \boldsymbol{B}_1^a\,, \tag{B.13}$$

$$\boldsymbol{C}^a \equiv \boldsymbol{A}_1^a + \boldsymbol{A}_2^a\,, \tag{B.14}$$

where the former, eq. (B.13), is often referred to as the "Lipatov vertex". Using this notation, it is possible to write the squared amplitude, after taking the medium average and summing over spins and colours, $\mathcal{P}_{\text{ant}}^{(1)}(k) \equiv \sum_\lambda \langle |\mathcal{M}_\lambda^{(1)}|^2 \rangle$, as

$$\mathcal{P}_{\text{ant}}^{(1)}(k) = 4g^4 C_A\, m_D^2 \int_{\boldsymbol{q}} \mathcal{V}^2(\boldsymbol{q}) \int_0^\infty \mathrm{d}x^+ n\left(x^+\right) \tilde{w}_{\text{ant}}^{(1)}\left(x^+; k, \boldsymbol{q}\right)\,, \tag{B.15}$$

where

$$\tilde{w}_{\text{ant}}^{(1)}\left(x^+;k,\boldsymbol{q}\right) = 2\left[1-\cos\frac{x^+}{\tau_1}\right]\boldsymbol{L}_1^a\cdot\boldsymbol{C}^a + 2\left[1-\cos\frac{x^+}{\tau_2}\right]\boldsymbol{L}_2^a\cdot\boldsymbol{C}^a$$
$$-2\left[1-\cos\frac{x^+}{\tau_{12}}\right]\boldsymbol{L}_1^a\cdot\boldsymbol{L}_2^a\,, \tag{B.16}$$

and $\tau_1 = 2k^+\big/\left(\boldsymbol{\kappa}_1-\boldsymbol{q}\right)^2$, $\tau_2 = 2k^+\big/\left(\boldsymbol{\kappa}_2-\boldsymbol{q}\right)^2$ and $\tau_{12} = \left(1/\tau_1 - 1/\tau_2\right)^{-1}$. While τ_1 and τ_2 are simply the formation times of a medium-induced gluon off either of the legs of the antenna, τ_{12} sets the time-scale for interference effects. Performing the colour decomposition, as given by eq. (B.9), allows us to write

$$\tilde{w}_{\text{ant}}^{(1)}\left(x^+;k,\boldsymbol{q}\right) = C_F\left[1-\cos\frac{x^+}{\tau_1}\right]\left(\boldsymbol{L}_1^2+\boldsymbol{A}_1^2-\boldsymbol{B}_1^2\right)$$
$$+C_A\bigg\{\left[1-\cos\frac{x^+}{\tau_2}\right]\left(\boldsymbol{L}_2^2+\boldsymbol{A}_2^2-\boldsymbol{B}_2^2-\boldsymbol{A}_1\cdot\boldsymbol{L}_2\right)$$
$$-\left[1-\cos\frac{x^+}{\tau_1}\right]\boldsymbol{A}_2\cdot\boldsymbol{L}_1+\left[1-\cos\frac{x^+}{\tau_{12}}\right]\boldsymbol{L}_1\cdot\boldsymbol{L}_2\bigg\}. \tag{B.17}$$

In order to make some sense out of this complicated expression, let us take the completely coherent scattering limit, i.e. $x^+\to\infty$. In that case we can neglect all the cosines, and eq. (B.17) reduces to

$$\lim_{x^+\to\infty}\tilde{w}_{\text{ant}}^{(1)}\left(x^+;k,\boldsymbol{q}\right) = C_F\left[\boldsymbol{L}_1^2+\boldsymbol{A}_1^2-\boldsymbol{B}_1^2\right]$$
$$+C_A\left[\boldsymbol{L}_2^2+\left(\boldsymbol{A}_2^2-\boldsymbol{A}_1\cdot\boldsymbol{A}_2\right)-\left(\boldsymbol{B}_2^2-\boldsymbol{B}_1\cdot\boldsymbol{B}_2\right)\right]\,. \tag{B.18}$$

Here we clearly see the expected features. In the medium, the Lipatov vertex gives rise to the Gunion-Bertsch spectrum, represented by $\boldsymbol{L}_i^2$. Secondly, the pure vacuum spectrum is affected by broadening, effectively replacing the vacuum spectrum with a broadened one with the appropriate weight. For the emission off the quark, since all interferences cancel, this is represented by $\boldsymbol{A}_1^2-\boldsymbol{B}_1^2$. For the emission off the gluon, due to the presence of the interference in the term proportional to C_A in eq. (B.12), we replace the complete vacuum contribution completely analogously. A similar systematic was found for the $q\bar{q}$ antenna in [62].

The analysis of the antenna spectrum has thus provided us with crucial information. Whenever the medium scattering takes place long after the gluon formation and interference times, we simply see that $\mathcal{C}^{(1)}$ subtracts a piece of the vacuum radiation from $\mathcal{C}^{(0)}$ with a proper weight (see eq. (B.15)) and replaces it with broadening. In addition to this, all colour charges radiate a Gunion-Bertsch spectrum. Naturally, in the general case, for finite scattering times we obtain a quite complicated interference pattern, eq. (B.17). This can however be used to be compared to the two gluon (one hard, one soft) emission off a quark analysed in this paper, where the antenna picture has to appear naturally in the situation where the formation time of the hard gluon is exactly zero.

References

[1] N. Armesto and E. Scomparin, *Heavy-ion collisions at the Large Hadron Collider: a review of the results from Run 1*, *Eur. Phys. J. Plus* **131** (2016) 52 [arXiv:1511.02151].

[2] J.D. Bjorken, *Energy loss of energetic partons in quark-gluon plasma: possible extinction of high p(t) jets in hadron-hadron collisions*, FERMILAB-PUB-82-059-THY (1982).

[3] ATLAS collaboration, *Observation of a centrality-dependent dijet asymmetry in lead-lead collisions at $\sqrt{s_{NN}} = 2.77$ TeV with the ATLAS detector at the LHC*, *Phys. Rev. Lett.* **105** (2010) 252303 [arXiv:1011.6182] [INSPIRE].

[4] CMS collaboration, *Observation and studies of jet quenching in PbPb collisions at nucleon-nucleon center-of-mass energy = 2.76 TeV*, *Phys. Rev.* **C 84** (2011) 024906 [arXiv:1102.1957] [INSPIRE].

[5] CMS collaboration, *Jet momentum dependence of jet quenching in PbPb collisions at $\sqrt{s_{NN}} = 2.76$ TeV*, *Phys. Lett.* **B 712** (2012) 176 [arXiv:1202.5022] [INSPIRE].

[6] CMS collaboration, *Studies of jet quenching using isolated-photon+jet correlations in PbPb and pp collisions at $\sqrt{s_{NN}} = 2.76$ TeV*, *Phys. Lett.* **B 718** (2013) 773 [arXiv:1205.0206] [INSPIRE].

[7] CMS collaboration, *Measurement of jet fragmentation into charged particles in pp and PbPb collisions at $\sqrt{s_{NN}} = 2.76$ TeV*, *JHEP* **10** (2012) 087 [arXiv:1205.5872] [INSPIRE].

[8] ATLAS collaboration, *Measurement of the jet radius and transverse momentum dependence of inclusive jet suppression in lead-lead collisions at $\sqrt{s_{NN}} = 2.76$ TeV with the ATLAS detector*, *Phys. Lett.* **B 719** (2013) 220 [arXiv:1208.1967] [INSPIRE].

[9] ATLAS collaboration, *Measurement of the Azimuthal Angle Dependence of Inclusive Jet Yields in Pb+Pb Collisions at $\sqrt{s_{NN}} = 2.76$ TeV with the ATLAS detector*, *Phys. Rev. Lett.* **111** (2013) 152301 [arXiv:1306.6469] [INSPIRE].

[10] CMS collaboration, *Modification of jet shapes in PbPb collisions at $\sqrt{s_{NN}} = 2.76$ TeV*, *Phys. Lett.* **B 730** (2014) 243 [arXiv:1310.0878] [INSPIRE].

[11] ALICE collaboration, *Measurement of charged jet suppression in Pb-Pb collisions at $\sqrt{s_{NN}} = 2.76$ TeV*, *JHEP* **03** (2014) 013 [arXiv:1311.0633] [INSPIRE].

[12] CMS collaboration, *Evidence of b-jet quenching in PbPb collisions at $\sqrt{s_{NN}} = 2.76$ TeV*, *Phys. Rev. Lett.* **113** (2014) 132301 [arXiv:1312.4198] [INSPIRE].

[13] CMS collaboration, *Measurement of jet fragmentation in PbPb and pp collisions at $\sqrt{s_{NN}} = 2.76$ TeV*, *Phys. Rev.* **C 90** (2014) 024908 [arXiv:1406.0932] [INSPIRE].

[14] ATLAS collaboration, *Measurement of inclusive jet charged-particle fragmentation functions in Pb+Pb collisions at $\sqrt{s_{NN}} = 2.76$ TeV with the ATLAS detector*, *Phys. Lett.* **B 739** (2014) 320 [arXiv:1406.2979] [INSPIRE].

[15] ATLAS collaboration, *Measurements of the nuclear modification factor for jets in Pb+Pb collisions at $\sqrt{s_{NN}} = 2.76$ TeV with the ATLAS detector*, *Phys. Rev. Lett.* **114** (2015) 072302 [arXiv:1411.2357] [INSPIRE].

[16] ALICE collaboration, *Measurement of jet suppression in central Pb-Pb collisions at $\sqrt{s_{NN}} = 2.76$ TeV*, *Phys. Lett.* **B 746** (2015) 1 [arXiv:1502.01689] [INSPIRE].

[17] CMS collaboration, *Nuclear modification factor of high transverse momentum jets in PbPb collisions at $\sqrt{s_{NN}} = 2.76$ TeV*, CMS-PAS-HIN-12-004 (2012).

[18] ALICE collaboration, *Measurement of jet quenching with semi-inclusive hadron-jet distributions in central Pb-Pb collisions at $\sqrt{s_{NN}} = 2.76\,TeV$*, *JHEP* **09** (2015) 170 [arXiv:1506.03984] [INSPIRE].

[19] PHENIX collaboration, S.S. Adler et al., *Suppressed π^0 production at large transverse momentum in central Au+Au collisions at $\sqrt{s_{NN}} = 200\,GeV$*, *Phys. Rev. Lett.* **91** (2003) 072301 [nucl-ex/0304022] [INSPIRE].

[20] STAR collaboration, J. Adams et al., *Transverse momentum and collision energy dependence of high p_T hadron suppression in Au+Au collisions at ultrarelativistic energies*, *Phys. Rev. Lett.* **91** (2003) 172302 [nucl-ex/0305015] [INSPIRE].

[21] M. Gyulassy and X.-n. Wang, *Multiple collisions and induced gluon Bremsstrahlung in QCD*, *Nucl. Phys.* **B 420** (1994) 583 [nucl-th/9306003] [INSPIRE].

[22] R. Baier, Y.L. Dokshitzer, A.H. Mueller, S. Peigne and D. Schiff, *Radiative energy loss of high-energy quarks and gluons in a finite volume quark-gluon plasma*, *Nucl. Phys.* **B 483** (1997) 291 [hep-ph/9607355] [INSPIRE].

[23] B.G. Zakharov, *Fully quantum treatment of the Landau-Pomeranchuk-Migdal effect in QED and QCD*, *JETP Lett.* **63** (1996) 952 [hep-ph/9607440] [INSPIRE].

[24] R. Baier, Y.L. Dokshitzer, A.H. Mueller and D. Schiff, *Medium induced radiative energy loss: equivalence between the BDMPS and Zakharov formalisms*, *Nucl. Phys.* **B 531** (1998) 403 [hep-ph/9804212] [INSPIRE].

[25] U.A. Wiedemann, *Gluon radiation off hard quarks in a nuclear environment: opacity expansion*, *Nucl. Phys.* **B 588** (2000) 303 [hep-ph/0005129] [INSPIRE].

[26] M. Gyulassy, P. Levai and I. Vitev, *Non-Abelian energy loss at finite opacity*, *Phys. Rev. Lett.* **85** (2000) 5535 [nucl-th/0005032] [INSPIRE].

[27] M. Gyulassy, P. Levai and I. Vitev, *Reaction operator approach to nonAbelian energy loss*, *Nucl. Phys.* **B 594** (2001) 371 [nucl-th/0006010] [INSPIRE].

[28] X.-N. Wang and X.-f. Guo, *Multiple parton scattering in nuclei: parton energy loss*, *Nucl. Phys.* **A 696** (2001) 788 [hep-ph/0102230] [INSPIRE].

[29] P.B. Arnold, G.D. Moore and L.G. Yaffe, *Photon and gluon emission in relativistic plasmas*, *JHEP* **06** (2002) 030 [hep-ph/0204343] [INSPIRE].

[30] S. Jeon and G.D. Moore, *Energy loss of leading partons in a thermal QCD medium*, *Phys. Rev.* **C 71** (2005) 034901 [hep-ph/0309332] [INSPIRE].

[31] S. Wicks, W. Horowitz, M. Djordjevic and M. Gyulassy, *Elastic, inelastic and path length fluctuations in jet tomography*, *Nucl. Phys.* **A 784** (2007) 426 [nucl-th/0512076] [INSPIRE].

[32] G.-Y. Qin, J. Ruppert, C. Gale, S. Jeon, G.D. Moore and M.G. Mustafa, *Radiative and collisional jet energy loss in the quark-gluon plasma at RHIC*, *Phys. Rev. Lett.* **100** (2008) 072301 [arXiv:0710.0605] [INSPIRE].

[33] J. Casalderrey-Solana and C.A. Salgado, *Introductory lectures on jet quenching in heavy ion collisions*, *Acta Phys. Polon.* **B 38** (2007) 3731 [arXiv:0712.3443] [INSPIRE].

[34] A. Majumder and M. Van Leeuwen, *The theory and phenomenology of perturbative QCD based jet quenching*, *Prog. Part. Nucl. Phys.* **66** (2011) 41 [arXiv:1002.2206] [INSPIRE].

[35] G. Ovanesyan and I. Vitev, *An effective theory for jet propagation in dense QCD matter: jet broadening and medium-induced bremsstrahlung*, *JHEP* **06** (2011) 080 [arXiv:1103.1074] [INSPIRE].

[36] Y. Mehtar-Tani, J.G. Milhano and K. Tywoniuk, *Jet physics in heavy-ion collisions*, *Int. J. Mod. Phys.* **A 28** (2013) 1340013 [`arXiv:1302.2579`] [ɪɴSPIRE].

[37] G.-Y. Qin and X.-N. Wang, *Jet quenching in high-energy heavy-ion collisions*, *Int. J. Mod. Phys.* **E 24** (2015) 1530014 [`arXiv:1511.00790`].

[38] I.P. Lokhtin et al., *Heavy ion event generator HYDJET++ (HYDrodynamics plus JETs)*, *Comput. Phys. Commun.* **180** (2009) 779 [`arXiv:0809.2708`] [ɪɴSPIRE].

[39] T. Renk, *Parton shower evolution in a* 3*D hydrodynamical medium*, *Phys. Rev.* **C 78** (2008) 034908 [`arXiv:0806.0305`] [ɪɴSPIRE].

[40] N. Armesto, L. Cunqueiro and C.A. Salgado, *Q-PYTHIA: a medium-modified implementation of final state radiation*, *Eur. Phys. J.* **C 63** (2009) 679 [`arXiv:0907.1014`] [ɪɴSPIRE].

[41] B. Schenke, C. Gale and S. Jeon, *MARTINI: an event generator for relativistic heavy-ion collisions*, *Phys. Rev.* **C 80** (2009) 054913 [`arXiv:0909.2037`] [ɪɴSPIRE].

[42] K.C. Zapp, J. Stachel and U.A. Wiedemann, *A local Monte Carlo framework for coherent QCD parton energy loss*, *JHEP* **07** (2011) 118 [`arXiv:1103.6252`] [ɪɴSPIRE].

[43] R.K. Ellis et al., *QCD and collider physics*, Cambridge University press, Cambridge U.K. (1996).

[44] J.-P. Blaizot, F. Dominguez, E. Iancu and Y. Mehtar-Tani, *Medium-induced gluon branching*, *JHEP* **01** (2013) 143 [`arXiv:1209.4585`] [ɪɴSPIRE].

[45] L. Apolinário, N. Armesto, J.G. Milhano and C.A. Salgado, *Medium-induced gluon radiation and colour decoherence beyond the soft approximation*, *JHEP* **02** (2015) 119 [`arXiv:1407.0599`] [ɪɴSPIRE].

[46] J.-P. Blaizot, E. Iancu and Y. Mehtar-Tani, *Medium-induced QCD cascade: democratic branching and wave turbulence*, *Phys. Rev. Lett.* **111** (2013) 052001 [`arXiv:1301.6102`] [ɪɴSPIRE].

[47] A. Kurkela and U.A. Wiedemann, *Picturing perturbative parton cascades in QCD matter*, *Phys. Lett.* **B 740** (2015) 172 [`arXiv:1407.0293`] [ɪɴSPIRE].

[48] R. Baier, A.H. Mueller, D. Schiff and D.T. Son, *'Bottom up' thermalization in heavy ion collisions*, *Phys. Lett.* **B 502** (2001) 51 [`hep-ph/0009237`] [ɪɴSPIRE].

[49] P.B. Arnold, G.D. Moore and L.G. Yaffe, *Effective kinetic theory for high temperature gauge theories*, *JHEP* **01** (2003) 030 [`hep-ph/0209353`] [ɪɴSPIRE].

[50] T. Liou, A.H. Mueller and B. Wu, *Radiative $p_\perp$-broadening of high-energy quarks and gluons in QCD matter*, *Nucl. Phys.* **A 916** (2013) 102 [`arXiv:1304.7677`] [ɪɴSPIRE].

[51] J.-P. Blaizot and Y. Mehtar-Tani, *Renormalization of the jet-quenching parameter*, *Nucl. Phys.* **A 929** (2014) 202 [`arXiv:1403.2323`] [ɪɴSPIRE].

[52] B. Wu, *Radiative energy loss and radiative $p_\perp$-broadening of high-energy partons in QCD matter*, *JHEP* **12** (2014) 081 [`arXiv:1408.5459`] [ɪɴSPIRE].

[53] E. Iancu, *The non-linear evolution of jet quenching*, *JHEP* **10** (2014) 095 [`arXiv:1403.1996`] [ɪɴSPIRE].

[54] J. Ghiglieri and D. Teaney, *Parton energy loss and momentum broadening at NLO in high temperature QCD plasmas*, *Int. J. Mod. Phys.* **E 24** (2015) 1530013 [`arXiv:1502.03730`].

[55] J. Ghiglieri, G.D. Moore and D. Teaney, *Jet-medium interactions at NLO in a weakly-coupled quark-gluon plasma*, `arXiv:1509.07773`.

[56] P. Arnold and S. Iqbal, *The LPM effect in sequential bremsstrahlung*, *JHEP* **04** (2015) 070 [*Erratum ibid.* **09** (2016) 072] [arXiv:1501.04964].

[57] M. Fickinger, G. Ovanesyan and I. Vitev, *Angular distributions of higher order splitting functions in the vacuum and in dense QCD matter*, *JHEP* **07** (2013) 059 [arXiv:1304.3497] [INSPIRE].

[58] Y. Mehtar-Tani, C.A. Salgado and K. Tywoniuk, *Anti-angular ordering of gluon radiation in QCD media*, *Phys. Rev. Lett.* **106** (2011) 122002 [arXiv:1009.2965] [INSPIRE].

[59] Y. Mehtar-Tani, C.A. Salgado and K. Tywoniuk, *Jets in QCD media: from color coherence to decoherence*, *Phys. Lett.* **B 707** (2012) 156 [arXiv:1102.4317] [INSPIRE].

[60] N. Armesto, H. Ma, Y. Mehtar-Tani, C.A. Salgado and K. Tywoniuk, *Coherence effects and broadening in medium-induced QCD radiation off a massive $q\bar{q}$ antenna*, *JHEP* **01** (2012) 109 [arXiv:1110.4343] [INSPIRE].

[61] J. Casalderrey-Solana and E. Iancu, *Interference effects in medium-induced gluon radiation*, *JHEP* **08** (2011) 015 [arXiv:1105.1760] [INSPIRE].

[62] Y. Mehtar-Tani, C.A. Salgado and K. Tywoniuk, *The radiation pattern of a QCD antenna in a dilute medium*, *JHEP* **04** (2012) 064 [arXiv:1112.5031] [INSPIRE].

[63] Y. Mehtar-Tani, C.A. Salgado and K. Tywoniuk, *The radiation pattern of a QCD antenna in a dense medium*, *JHEP* **10** (2012) 197 [arXiv:1205.5739] [INSPIRE].

[64] J. Casalderrey-Solana and A. Ficnar, *Holographic three-jet events in strongly coupled $N = 4$ Yang-Mills plasma*, arXiv:1512.00371.

[65] J. Casalderrey-Solana, Y. Mehtar-Tani, C.A. Salgado and K. Tywoniuk, *New picture of jet quenching dictated by color coherence*, *Phys. Lett.* **B 725** (2013) 357 [arXiv:1210.7765] [INSPIRE].

[66] R.B. Neufeld and I. Vitev, *The Z^0-tagged jet event asymmetry in heavy-ion collisions at the CERN Large Hadron Collider*, *Phys. Rev. Lett.* **108** (2012) 242001 [arXiv:1202.5556] [INSPIRE].

[67] W. Dai, I. Vitev and B.-W. Zhang, *Momentum imbalance of isolated photon-tagged jet production at RHIC and LHC*, *Phys. Rev. Lett.* **110** (2013) 142001 [arXiv:1207.5177] [INSPIRE].

[68] J. Huang, Z.-B. Kang and I. Vitev, *Inclusive b-jet production in heavy ion collisions at the LHC*, *Phys. Lett.* **B 726** (2013) 251 [arXiv:1306.0909] [INSPIRE].

[69] Z.-B. Kang, R. Lashof-Regas, G. Ovanesyan, P. Saad and I. Vitev, *Jet quenching phenomenology from soft-collinear effective theory with Glauber gluons*, *Phys. Rev. Lett.* **114** (2015) 092002 [arXiv:1405.2612] [INSPIRE].

[70] Y.T. Chien and I. Vitev, *Towards the understanding of jet shapes and cross sections in heavy ion collisions using soft-collinear effective theory*, *JHEP* **05** (2016) 023 [arXiv:1509.07257] [INSPIRE].

[71] G.Y. Qin, A. Majumder, H. Song and U. Heinz, *Energy and momentum deposited into a QCD medium by a jet shower*, *Phys. Rev. Lett.* **103** (2009) 152303 [arXiv:0903.2255] [INSPIRE].

[72] G.-Y. Qin, *Parton shower evolution in medium and nuclear modification of photon-tagged jets in Pb+Pb collisions at the LHC*, *Eur. Phys. J.* **C 74** (2014) 2959 [arXiv:1210.6610] [INSPIRE].

[73] C. Young, B. Schenke, S. Jeon and C. Gale, *Dijet asymmetry at the energies available at the CERN Large Hadron Collider*, *Phys. Rev.* **C 84** (2011) 024907 [arXiv:1103.5769] [INSPIRE].

[74] T. Renk, *On the sensitivity of the dijet asymmetry to the physics of jet quenching*, *Phys. Rev.* **C 85** (2012) 064908 [arXiv:1202.4579] [INSPIRE].

[75] X.-N. Wang and Y. Zhu, *Medium modification of γ-jets in high-energy heavy-ion collisions*, *Phys. Rev. Lett.* **111** (2013) 062301 [arXiv:1302.5874] [INSPIRE].

[76] Y. Mehtar-Tani and K. Tywoniuk, *Jet (de)coherence in Pb-Pb collisions at the LHC*, *Phys. Lett.* **B 744** (2015) 284 [arXiv:1401.8293] [INSPIRE].

[77] Y. Mehtar-Tani, *Relating the description of gluon production in pA collisions and parton energy loss in AA collisions*, *Phys. Rev.* **C 75** (2007) 034908 [hep-ph/0606236] [INSPIRE].

[78] M. Sjödahl, *ColorMath — A package for color summed calculations in* SU(*NC*), *Eur. Phys. J.* **C 73** (2013) 2310 [arXiv:1211.2099] [INSPIRE].

[79] J.F. Gunion and G. Bertsch, *Hadronization by color bremsstrahlung*, *Phys. Rev.* **D 25** (1982) 746 [INSPIRE].